AGU PUBLICATIONS

JGR

Journal of Geophysical Research: Space Physics

RESEARCH ARTICLE
10.1002/2016JA023367

This article is a companion to *Thomsen et al.* [2017] doi: 10.1002/2016JA023368.

Key Points:
- We model the modulations of Saturn's tail current sheet due to the fields of the northern and southern planetary period oscillations (PPOs)
- North-south sheet oscillations maximize when the two PPO systems are in phase and thickness modulations when they are in antiphase
- Sawtooth waveforms occur at intermediate relative phases with opposite senses either side of antiphase maximizing for equal PPO amplitudes

Correspondence to:
S. W. H. Cowley,
swhc1@ion.le.ac.uk

Citation:
Cowley, S. W. H., G. Provan, G. J. Hunt, and C. M. Jackman (2017), Planetary period modulations of Saturn's magnetotail current sheet: A simple illustrative mathematical model, *J. Geophys. Res. Space Physics*, *122*, 258–279, doi:10.1002/2016JA023367.

Received 19 AUG 2016
Accepted 8 OCT 2016
Accepted article online 6 DEC 2016
Published online 19 JAN 2017

Planetary period modulations of Saturn's magnetotail current sheet: A simple illustrative mathematical model

S. W. H. Cowley[1], G. Provan[1], G. J. Hunt[1], and C. M. Jackman[2]

[1]Department of Physics and Astronomy, University of Leicester, Leicester, UK, [2]Department of Physics and Astronomy, University of Southampton, Southampton, UK

Abstract We mathematically model the modulation effects on Saturn's equatorial magnetotail and magnetodisk current sheet produced by the combined magnetic field perturbations of the northern and southern planetary period oscillation (PPO) systems, specifically north-south displacements associated with the radial perturbation field and thickness modulations associated with the colatitudinal perturbation field. Since the phasing of the two PPO systems is taken to be related to the radial field perturbations, while the relative phasing of the colatitudinal perturbations is opposite for the two systems, the north-south oscillations reinforce when the two PPO systems are in phase, while the thickening-thinning effects reinforce when they are in antiphase. For intermediate relative phases we show that when the northern PPO system leads the southern the sheet is thicker when moving south to north than when moving north to south, while when the northern PPO system lags the southern the sheet is thicker when moving north to south than when moving south to north, thus leading to sawtooth profiles in the radial field for near-equatorial observers, of opposite senses in the two cases. Given empirically determined modulation amplitudes, the maximum sawtooth effect is found to be small when one system dominates the other, but becomes clear when the amplitude of one system lies within a factor of 2 of the other.

1. Introduction

A major feature of Saturn's magnetosphere is the occurrence of ubiquitous modulations near the ~10.6 h planetary rotation period, despite the close axisymmetry of the planet's internally generated magnetic field [*Burton et al.*, 2010]. These modulations, termed "planetary period oscillations" (PPOs), are observed not only in the magnetic field [e.g., *Espinosa and Dougherty*, 2000; *Cowley et al.*, 2006; *Southwood and Kivelson*, 2007; *Andrews et al.*, 2010a] but also in the plasma and energetic particle populations [e.g., *Carbary and Krimigis*, 1982; *Carbary et al.*, 2007, 2008a; *Burch et al.*, 2009], plasma waves [e.g., *Gurnett et al.*, 2009b; *Wang et al.*, 2010; *Ye et al.*, 2010], auroral ultraviolet emissions [e.g., *Sandel and Broadfoot*, 1981; *Sandel et al.*, 1982; *Nichols et al.*, 2008, 2010a, 2010b], and kilometer-band auroral radio emissions [e.g., *Warwick et al.*, 1981, 1982; *Desch and Kaiser*, 1981; *Gurnett et al.*, 2005]. Long-term studies of these auroral radio emissions, termed Saturn kilometric radiation (SKR), have shown that two such modulation periods are usually present, one associated with the northern hemisphere and the other with the southern, and that these periods can vary by up to ~1% per Earth year associated with Saturn's seasons [*Galopeau and Lecacheux*, 2000; *Kurth et al.*, 2008; *Gurnett et al.*, 2009a, 2010, 2011; *Lamy*, 2011; *Cowley et al.*, 2016]. These northern and southern systems are also manifest in magnetic field data, where each system produces a quasi-uniform perturbation field in the equatorial plane that rotates with the corresponding SKR period, which closes individually in a rotating quasi-dipolar perturbation field over the corresponding planetary pole [*Provan et al.*, 2009, 2011; *Andrews et al.*, 2010b]. The equatorial field perturbations thus consist of the vector sum of the contributions from the two PPO systems, varying at the beat period of the two oscillations, while the polar perturbations are found to be pure northern or southern to within an ~10% measurement limit by amplitude [*Andrews et al.*, 2012; *Provan et al.*, 2013; *Hunt et al.*, 2015].

In this paper we consider the modulation effects of these PPO-related perturbation fields on the magnetotail and magnetodisk current sheets formed in Saturn's equatorial region, and how these depend on the amplitudes of the two systems and their relative phase. In Figure 1 we begin by providing some background on PPO properties derived over the Cassini mission to date, together with orbit data that are relevant to the availability of current sheet observations, particularly those on the nightside in the magnetotail. The plot

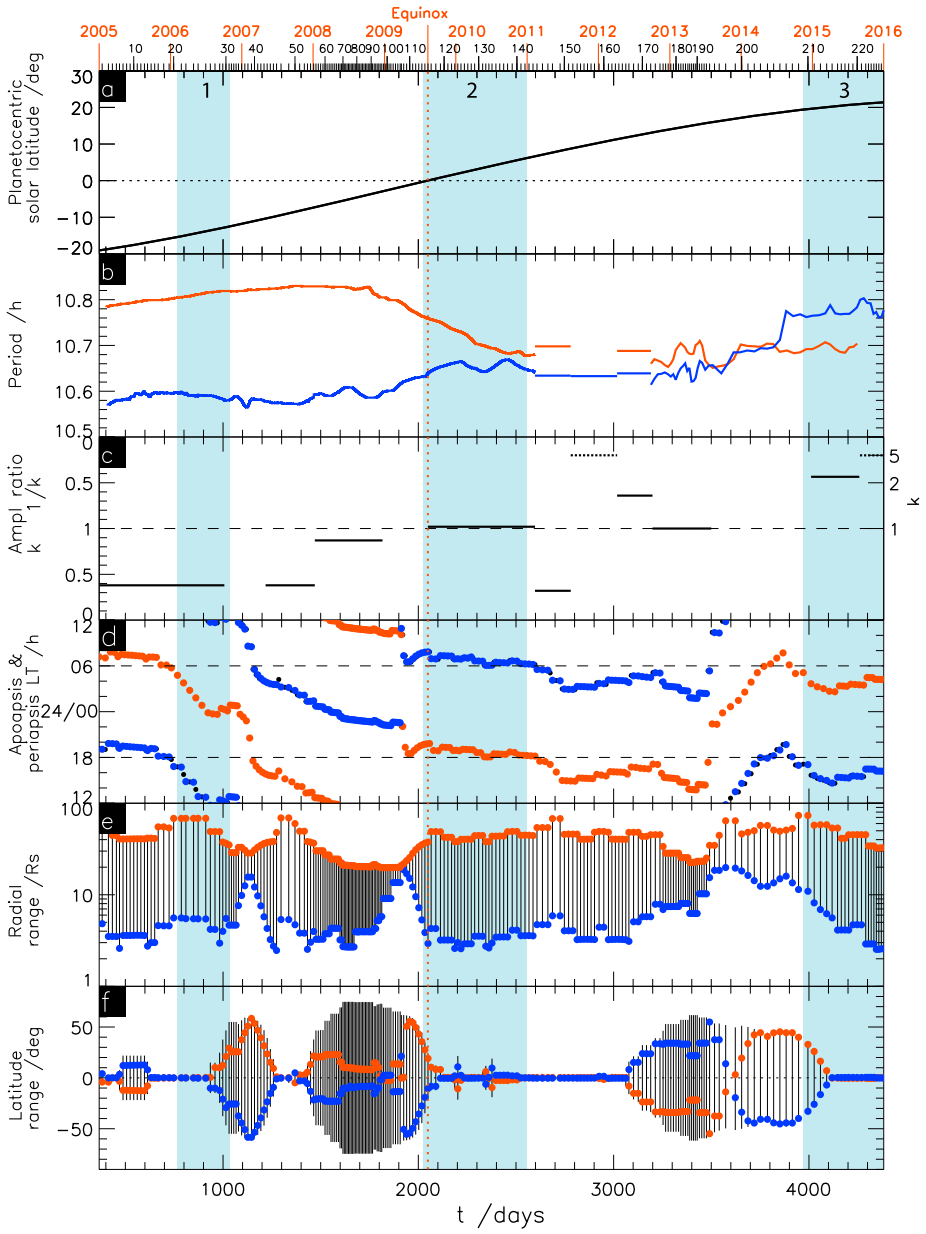

Figure 1. Plot showing Saturn season, PPO, and Cassini orbit data over calendar years 2005–2015 inclusive, i.e., for $t = 366 - 4383$ days where $t = 0$ corresponds to 00:00 UT on 1 January 2004, as shown at the bottom of the plot. Year boundaries are shown in red at the top of the plot, together with Cassini Rev numbers plotted at the time of periapsis. (a) Tthe planetocentric latitude of the Sun at Saturn, passing through zero at vernal equinox on 11 August 2009, marked at the top of the plot and by the vertical dotted red line. (b) The northern (blue) and southern (red) PPO periods derived from magnetic field oscillation phase data by *Andrews et al.* [2012] and *Provan et al.* [2013, 2014, 2016]. (c) Corresponding piecewise values of the north/south amplitude ratio k of the two systems determined from dual-phase modulations observed in quasi-dipolar core region (dipole $L \leq 12$) data when available, where the horizontal dashed line indicates $k = 1$ (equal amplitudes), with k itself being shown between zero and unity in the lower half plot, while $1/k$ is similarly shown between unity and zero in the upper half plot, thus spanning the whole range of k from zero to infinity (k scale is also shown on the right-hand axis for the upper part of the panel). The dotted lines at $1/k = 0.2$ indicate intervals in which no southern modulations were detected in the core region indicating $k \geq 5$ (i.e., $1/k \leq 0.2$). (d) The LT of apoapsis (red) and periapsis (blue) plotted at the times of apoapsis and periapsis, respectively, where the LT scale is shown centered at midnight (24/00 h LT) with the horizontal dashed lines indicating the central LT band between 18 and 06 h via midnight for which apoapsis is located on the planet's nightside. (e) The radial range on each Rev on a log scale, plotted as a vertical bar at the time of periapsis. (f) The latitude range on each Rev, also plotted as a vertical bar at the time of periapsis, with the latitudes of apoapsis (red) and periapsis (blue) marked. The blue bars, numbered at the top of the plot, indicate three principal seasons of Cassini orbits during which near-equatorial Saturn tail data are available extending to radial distances of at least a few tens of R_S.

spans calendar years 2005–2015 inclusive, i.e., the interval $t = 366 - 4383$ days, where $t = 0$ corresponds to 00:00 UT on 1 January 2004 (the effective approach phase start date of the Cassini mission at Saturn). Year boundaries are shown at the top of the plot, together with Cassini orbit revolution (Rev) numbers, defined from apoapsis to apoapsis and plotted at the time of periapsis. Figure 1a first shows the planetocentric latitude of the Sun at Saturn, indicative of Saturn's season. The interval began during southern summer, ~2.2 (Earth) years after southern solstice in October 2002, and ended during northern spring, ~1.4 years before northern solstice in May 2017. Vernal equinox, when the solar latitude passed through zero, occurred on 11 August 2009, as marked at the top of the plot and by the vertical dotted red line.

Figure 1b shows the northern (blue) and southern (red) PPO periods, specifically those derived from magnetic field oscillation data by *Andrews et al*. [2012] for 2005 to 2010 inclusive, *Provan et al*. [2013, 2014] for 2011 to 2012, and *Provan et al*. [2016] for 2013 to 2015. PPO periods have also been derived near-continuously from SKR modulation data and generally show good agreement with these magnetic field values [e.g., *Lamy*, 2011; *Provan et al*., 2014, 2016; *Cowley and Provan*, 2015, 2016]. These data show that the two periods were initially well separated under southern summer conditions, ~10.6 h for the northern system and ~10.8 h for the southern, but converged toward a common period ~10.7 h over an ~2 (Earth) year interval centered near equinox. After briefly near-coalescing in 2010, the two periods separated again with the northern ~10.64 h remaining a little shorter than the southern ~10.69 h, before finally coalescing at ~10.66 h in mid-2013. The joint periods then drifted together to ~10.70 h over the following year, after which the northern period separated from the near-constant southern period and increased to ~10.78 h by the end of 2015, resulting in the first enduring reversal of the northern and southern periods during the Cassini era.

Figure 1c shows piecewise values of the north/south amplitude ratio of the two systems k, determined from the phase modulations of the field oscillations observed in the quasi-dipolar "core" region of the magnetosphere (dipole $L \leq 12$), when available. The lower half plot shows k itself for values between zero and unity (dashed line) corresponding to southern-dominant oscillations, while the upper half plot shows $1/k$ for values between unity and zero corresponding to northern-dominant oscillations, thus covering the whole range of k from zero to infinity. These data show that the southern oscillations were dominant with $k \approx 0.38$ during the southern summer interval to ~2007, following which the northern amplitude doubled while the southern amplitude modestly declined to produce near-equal values over a 3 (Earth) year interval centered near equinox, with $k \approx 0.87$ during 2008 and $k \approx 1.02$ between mid-2009 and the end of 2010. The amplitude ratio then underwent a sequence of abrupt transitions at ~200 day intervals between early 2011 and mid-2013 before returning to values near unity between mid-2012 and mid-2013. Core region data were not available during the interval of PPO period coalescence in 2013 and 2014, but when these data resumed in early 2015 after the reversal of northern and southern periods, the northern oscillations were found to be dominant with $k \approx 2.3$ (i.e., $1/k \approx 0.44$), thus mirroring preequinox conditions during southern summer near the beginning of the Cassini mission. By the end of 2015, however, the ratio had increased further to $k > 5$ (as indicated by the dotted line), meaning that the effect of the southern oscillations could not then be discerned in the core equatorial field data.

In Figures 1d–1f we show Cassini orbit data germane to the availability of in situ observations of current sheet modulations in Saturn's tail. To observe such effects the spacecraft apoapsis should be located on the nightside of the planet at radial distances of at least a few tens of Saturn radii (R_s, Saturn's 1 bar equatorial radius, equal to 60,268 km), with near-equatorial orbits preferred since highly inclined orbits generally make only a single clear crossing through the sheet structure. We note that other factors may play a role to further limit the availability of suitable data, such as the seasonal warping of the current sheet center away from the planetary equatorial plane [*Arridge et al*., 2008], but the above criteria provide a useful initial guide. Figure 1d thus shows the local time (LT) of apoapsis (red) and periapsis (blue) plotted at the times of apoapsis and periapsis, respectively, where the LT scale is centered at midnight (24/00 h LT) with the horizontal dashed lines indicating the central LT band between 18 and 06 h for which apoapsis (red) is located on the nightside. Figure 1e then shows the radial range on each Rev on a log scale, plotted as a vertical bar at the time of periapsis, while Figure 1f shows the latitude range on each Rev, also plotted as a vertical bar at the time of periapsis, with the latitudes of apoapsis (red) and periapsis (blue) marked. Examination of these data indicates that three main seasons of tail observations are available for study, occurring during 2006 (Revs 21 to 31), mid-2009 to end 2010 (Revs 115 to 142), and 2015 (Revs 210 to 228), which are marked in Figure 1 by the

vertical blue bars. It can be seen that these three seasons, as numbered at the top of the plot, occurred under southern-dominant ($k \approx 0.38$), near-equal ($k \approx 1.0$), and northern-dominant ($k \approx 2.3$) PPO conditions, respectively. These k values will thus be employed in later sections in the model evaluations presented.

With this introduction to observed PPO properties and Cassini tail data availability, we now briefly review observations of PPO-related modulations of Saturn's equatorial magnetotail and magnetodisk plasma and/or current sheet during the Cassini mission. Such modulations were first reported by *Carbary et al*. [2008b] in Cassini energetic neutral atom image data obtained in late 2004, showing oscillatory tilting of the plasma sheet related to the then-dominant southern SKR modulation phase. *Morooka et al*. [2009] also investigated plasma density data obtained by the Cassini RPWS Langmuir probe showing the presence of density modulations in the magnetotail and magnetodisk plasma sheet near the planetary rotation period. Using data obtained between mid-2004 and mid-2007 when the southern PPO was dominant (Figure 1c), they found that the density variations were best modeled through a combination of oscillations in the north-south position of the center of the plasma sheet, together with periodic thickening and thinning, such that the plasma layer was thicker and more dense when displaced to the south of its mean position, and thinner and less dense when displaced to the north. *Jackman et al*. [2009] also reported the occurrence of periodic reversals in the radial component of the magnetic field during the 2006 season of Saturn tail data (interval 1 in Figure 1), showing the presence of PPO-related north-south displacements of the current sheet together with related plasma density and temperature modulations.

These tail field and related plasma modulations were subsequently modeled by *Arridge et al*. [2011] in relation to the then-dominant southern PPO magnetic phases determined from the near-equatorial core region field perturbations by *Andrews et al*. [2008]. The results showed that the current sheet was displaced to the south of its mean position when the equatorial perturbation field pointed radially outward at the LT of the observation and was displaced to the north when the equatorial perturbation field pointed radially inward. The north-south motions were described as an oscillatory tilting of the sheet center through an angle of amplitude $\pm 12°$ hinging at a cylindrical radial distance of 12 R_s, such that the displacements were ~ ± 4 R_s at typical observed distances of a few tens of R_s down-tail. These relations with the perturbation fields in the core were found to hold only for data from the southern tail, however, and broke down for data obtained in the north.

Provan et al. [2012], examining these same 2006 tail data, showed that while the perturbations in the southern tail were indeed modulated at the dominant southern period, those in the northern tail were modulated at the northern PPO period, thus accounting for the breakdown found by *Arridge et al*. [2011]. The region of the central current sheet, however, was found to be dual-modulated by both systems, though as expected, the southern was the strongest during the interval they examined. The form of the modulations was further shown to depend on the relative phase of the two PPO systems, principally involving north-south displacements when the two PPO systems were in phase, to the south when the two core perturbation fields pointed radially outward at the LT of the observations and to the north when these perturbation fields pointed radially inward, similar to the results obtained by *Arridge et al*. [2011]. These motions were also found to be combined with thickness modulations when the two systems were in antiphase, the current sheet being thicker when displaced to the south with the dominant southern perturbation field pointing radially outward and the weaker antiphase northern perturbation field pointing radially inward, and thinner when it was displaced to the north with the dominant southern perturbation field pointing radially inward and the weaker northern perturbation field pointing radially outward. These variations thus had the same sense as the related displacement-thickness modulations reported in plasma sheet data over ~2004–2007 by *Morooka et al*. [2009].

Modulations of the tail plasma sheet have also been reported in a magnetohydrodynamic simulation study by *Jia and Kivelson* [2012], in which magnetospheric oscillations were induced by imposing rotating twin-vortex flows in the two polar ionospheres, which drive rotating systems of field-aligned currents outward into the magnetosphere. The two systems were taken to rotate with slightly differing periods, such that the modulations due to the two sources go in and out of phase at the beat period during the course of the simulation, with the northern perturbations being a factor of 3 weaker than the southern, corresponding approximately to southern summer conditions during tail interval 1 in Figure 1. In conformity with the results of *Arridge et al*. [2011] and *Provan et al*. [2012], the resulting north-south oscillations of the plasma sheet (specifically at ~40 R_s down-tail) were shown to maximize when the two perturbation systems were in phase and to minimize when

in antiphase, while conversely, the thickness modulations were found to maximize when in antiphase and to minimize when in phase.

Szego et al. [2013] have also studied the north-south displacements of the nightside plasma and current sheet during near-equinoctial conditions in the 2009–2010 tail season (interval 2 in Figure 1), for which the amplitudes of the two systems are near equal. Accordingly, they employed a modified version of the *Arridge et al*. [2011] model, which incorporates the summed effect of both northern and southern systems, and found good agreement with the observed plasma and current sheet center crossings for a north/south displacement amplitude ratio of ~0.95.

Most recently *Thomsen et al*. [2017] have reported discovery of a new feature in the PPO-related perturbations of Saturn's nightside current sheet, also observed in tail data from 2010 (within interval 2 in Figure 1). On some nightside spacecraft passes the south-to-north field transitions occur consistently more slowly than the subsequent north-to-south transitions, thus giving rise to a "sawtooth" waveform in the primary radial field component. On other passes the asymmetry was reversed, giving rise to a sawtooth waveform of the opposite sense, while on still others the effect was essentially absent. Such effects were not found to be clearly evident in the earlier 2006 tail data, however. In this paper we consider these effects and provide a simple physical discussion and mathematical model of PPO-related modulations in Saturn's magnetotail and magnetodisk, showing how they can result from the combined effect of the northern and southern PPO systems under differing conditions of relative phase and relative amplitude. In section 2 we provide a simple physical discussion of PPO-related modulations of the equatorial current sheet, while in section 3 we derive a simple mathematical model which demonstrates the above effects, with illustrative examples presented in section 4.

2. Theoretical Picture

A simple physical explanation of these variations in the north-south position and thickness of the current sheet can be obtained by considering the magnetic perturbations associated with the rotating northern and southern PPO current systems illustrated in Figure 2 [*Andrews et al*., 2010a; *Provan et al*., 2012; *Jackman et al*., 2016]. Figures 2a and 2c show the form of the PPO perturbation fields in a principal meridian for the northern and southern systems, respectively, where the black arrowed lines indicate the background magnetospheric field, to a first approximation axisymmetric about the central north-south rotation axis, and the blue and red arrowed lines indicate the respective PPO perturbation fields. As indicated in section 1, these perturbation fields consist of a quasi-uniform field in the equatorial region pointing from left to right as drawn, which closes in a quasi-dipolar field over the corresponding pole. The effective magnetic dipole associated with the quasi-dipolar field is in the same direction as the quasi-uniform equatorial field, transverse to the planetary dipole and spin axis, also directed from left to right in these figures. The two perturbation field systems then rotate with time independently at the northern and southern PPO periods, respectively, in the sense of planetary rotation. The circulation sense of the field perturbations requires a current flowing out of the plane of the diagram in Figure 2a and into the plane of the diagram in Figure 2c, flowing along field lines into the ionosphere on one side of the polar region and out on the other, and closing principally in the magnetosphere where it produces a rotating force on the plasma. It is the magnetic moment of this current system that forms the rotating transverse magnetic dipole indicated above.

Azimuthal position with respect to these current-field systems is given by phase angles $\Psi_{N,S}$ for the northern (N) and southern (S) PPO systems, respectively, where $\Psi_{N,S} = 0°$ corresponds to the meridian where the quasi-uniform equatorial field points radially outward from the planet, on the right side in both Figures 2a and 2c as marked, and $\Psi_{N,S} = 180°$ to the meridian where the quasi-uniform equatorial field points radially inward on the opposite side of the planet, on the left side in Figures 2a and 2c as also marked. The values of $\Psi_{N,S}$ then increase clockwise around the planet at any instant of time as viewed from the north, such that at a fixed position their values increase steadily with time as the PPO system rotates near the planetary rotation period, by 360° for a full rotation.

The effects of these perturbations on the overall current sheet fields away from the planet are indicated schematically in Figures 2b and 2d for the northern and southern systems, respectively, where for economy of drawing we again represent conditions for $\Psi_{N,S}$ equal to 0° and 180° on opposite sides of the planet as

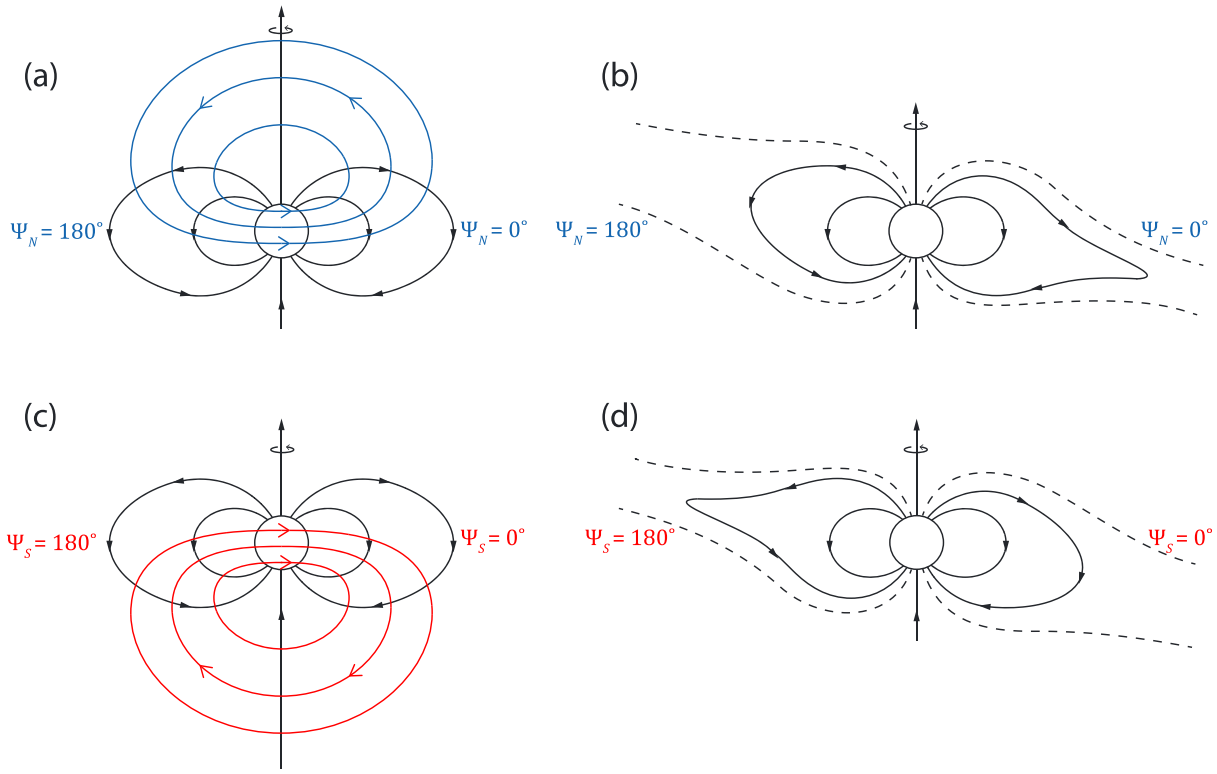

Figure 2. Sketches showing the form of the perturbation fields associated with the PPO current systems and the plasma and current sheet effects to which they give rise. (a) The form of the perturbation field lines for the northern PPO system in the prime $\Psi_N = 0° - 180°$ meridian as indicated (arrowed blue lines), together with the near axisymmetric undisturbed background field (arrowed black lines). The planetary spin axis is directed vertically upward as indicated. (b) The expected form of the resulting modulations of the outer magnetodisk and tail current sheet contained between the pairs of dashed lines, namely, a thinner current sheet displaced south of its mean position at $\Psi_N = 0°$, and a thicker current sheet displaced north of its mean position at $\Psi_N = 180°$. (c) The form of the perturbation field lines for the southern PPO system in the prime $\Psi_S = 0° - 180°$ meridian as indicated (arrowed red lines), in the same format as Figure 2a. (d) The expected form of the resulting modulations of the outer magnetodisk and tail current sheet, namely, a thicker current sheet displaced south of its mean position at $\Psi_S = 0°$, and a thinner current sheet displaced north of its mean position at $\Psi_S = 180°$. (Adapted from *Andrews et al.* [2010b] and *Provan et al.* [2012].)

marked, as in Figures 2a and 2c, though in this paper these are applied principally to conditions in the near-tail region on the nightside of the planet. It can first be seen that the radially outward quasi-uniform perturbation field at $\Psi_{N,S} = 0°$ adds to the current sheet field north of the equator and subtracts from the current sheet field south of the equator (on the right of these diagrams), while the radially inward field at $\Psi_{N,S} = 180°$ subtracts from the current sheet field north of the equator and adds to the current sheet field south of the equator (on the left of these diagrams). Bearing in mind that quasi-static magnetic pressure balance must be maintained across these current sheets, the implication is that the sheet will be displaced to the south at $\Psi_{N,S} = 0°$ and to the north at $\Psi_{N,S} = 180°$ as shown in both Figures 2b and 2d, thus producing characteristic PPO-periodic oscillations in the principal radial component of the tail magnetic field and plasma as these systems rotate with time, as reported, e.g., by *Jackman et al.* [2009]. These displacements are also those expected from the tilt in the overall magnetic equator resulting from the vector addition of the planetary dipole directed vertically upward, and the rotating PPO-related transverse dipole pointing from left to right in Figures 2a and 2c. The sense of the observed oscillations is indeed consistent with Figures 2b and 2d, determined principally by the southern PPO system in preequinox southern summer data [*Carbary et al.*, 2008b; *Arridge et al.*, 2011; *Provan et al.*, 2012], but by the combined action of near-equal northern and southern systems in later near-equinoctial data [*Szego et al.*, 2013]. The inferred oscillations at distances of a few tens of R_s down-tail are ~4 R_s in amplitude as indicated in section 1, comparable with the overall width of the current sheet, but with larger combined oscillations when the two PPO systems are in phase with each other than when they are in antiphase.

In addition to the north-south displacements, however, it can be seen that the colatitudinal perturbation fields of the PPO systems add to the planetary background field on one side of the planet, at $\Psi_N = 180°$ for

the northern system in Figure 2a and at $\Psi_S = 0°$ for the southern system in Figure 2c, but subtract from the background field on the other side of the planet, at $\Psi_N = 0°$ for the northern system in Figure 2a and at $\Psi_S = 180°$ for the southern system in Figure 2c. Increasing the near-equatorial field threading the current sheet results in the field lines becoming less stretched out away from the planet, leading to a thicker current sheet (bounded by the dashed lines in Figures 2b and 2d), while reducing the field threading the current sheet results in the field lines becoming more stretched out away from the planet, leading to a thinner current sheet. For the northern system in Figure 2b, for which the radial and colatitudinal perturbation fields are in antiphase in Figure 2a, this results in a thinner current sheet when it is displaced to the south at $\Psi_N = 0°$ and a thicker current sheet when it is displaced to the north at $\Psi_N = 180°$. For the southern system in Figure 2d, however, for which the radial and colatitudinal perturbation fields are instead in phase in Figure 2c, this results in a thicker current sheet when it is displaced to the south at $\Psi_S = 0°$ and a thinner current sheet when it is displaced to the north at $\Psi_S = 180°$. The sense of these thickness variations relative to the north-south displacement is consistent with the findings of *Morooka et al*. [2009] specifically for the preequinox southern-dominant PPO conditions they studied, with variations in thickness which were a significant fraction of the whole. It is also consistent with the finding of *Provan et al*. [2012] of significant thickening and thinning of the current sheet under antiphase conditions of the two PPO systems, when the effects of the two systems reinforce each other. The opposite behavior of the thickening and thinning of the current sheet relative to the north-south displacement in the two PPO systems, resulting from the opposite relative phasing of the radial and colatitudinal perturbation fields of the two systems, is a critical feature in the following discussion.

As mentioned above, the overall PPO-related perturbations observed in the near-equatorial current sheet field will evidently depend on the combined action of both northern and southern PPO systems, and thus on their relative phasing. As evident from Figures 2b and 2d, when the two systems are in phase, $\Psi_N = \Psi_S$ modulo 360°, the north-south displacements of the two systems will reinforce each other, while the thickening and thinning effects will tend to cancel. However, when the two systems are in antiphase a half beat period later, $\Psi_N = \Psi_S + 180°$ modulo 360°, the thickening and thinning effects will reinforce each other, while the north-south displacements will tend to cancel. If we can treat the combined effect of the two systems as approximately additive, then for near-equal amplitudes of the two systems, for example, when the two systems are in phase the north-south oscillation amplitude will be approximately doubled, while the thickening and thinning modulations will approximately cancel, while when they are in antiphase the thickening and thinning modulations will be approximately doubled and the north-south oscillation amplitude will approximately cancel, in agreement with the results of *Szego et al*. [2013] with regard to the north-south oscillation effect. Even when one system is only ~40% of the amplitude of the other, as appropriate to the postsolstice southern summer conditions, the ratio of the maximum to minimum amplitudes of these effects will be $\sim (1 + 0.4)/(1 - 0.4)) \approx 2.3$, compatible with the results of *Provan et al*. [2012] for the thickening and thinning effect. Effects associated with intermediate phase differences of the two systems, however, are less obvious, have not been explored previously, and are now the subject of discussion through the development of a simple mathematical model.

3. Simple Mathematical Model

We focus on the principal radial field component that reverses sign across the tail current sheet, and for simplicity express this as a hyperbolic tangent function of north-south position z, given by

$$\frac{B_r(z,\ \Psi_N,\ \Psi_S)}{B_o} = \tanh\left[\frac{z - z^*(\Psi_N,\ \Psi_S)}{D^*(\Psi_N,\ \Psi_S)}\right], \tag{1a}$$

where B_o is the lobe field strength on either side of the current sheet, z^* is the displacement of the center of the sheet from the mean position $z = 0$ depending on both northern and southern PPO phases $\Psi_{N,S}$, and D^* is the half-width of the current sheet which also depends on both northern and southern PPO phases $\Psi_{N,S}$. Note that at north-south distances $z = z^* \pm D^*$ we have $\tanh[(z - z^*)/D^*] = \tanh[\pm 1] \approx \pm 0.76$ compared with peak positive and negative values at large positive and negative z of $\tanh[\pm\infty] = \pm 1$. As in *Arridge et al*. [2011], a corresponding illustrative model for the plasma number density N based on the Harris neutral

sheet model (for which the field varies with z as in equation (1a)) can similarly be constructed by using the function

$$\frac{N(z,\ \Psi_N,\ \Psi_S)}{N_o} = \mathrm{sech}^2\left[\frac{z - z^*(\Psi_N,\ \Psi_S)}{D^*(\Psi_N,\ \Psi_S)}\right]. \tag{1b}$$

Here N_o is the peak number density at the center of the current sheet at $z = z^*$, with the normalized density then falling to $\mathrm{sech}^2[(z - z^*)/D^*] = \mathrm{sech}^2[\pm 1] \approx 0.42$ at $z = z^* \pm D^*$, and to near-zero values at large positive and negative values of z ($\mathrm{sech}^2[\pm\infty] = 0$). Pressure balance between the center of the current sheet and the lobes requires $N_o k_B T \approx B_o^2/2\mu_o$, where k_B is Boltzmann's constant and T is the temperature of the plasma sheet plasma, and where we have assumed that the field pressure at the sheet center is small compared with that in the lobes. We thus see that N_o can be taken to be an approximate constant during the oscillations provided that the lobe field strength B_o and the plasma sheet temperature T are also approximate constants.

Considering the PPO phase dependence of the current sheet displacements in Figure 2 we may then write

$$z^*(\Psi_N,\ \Psi_S) = -(z_N \cos\Psi_N + z_S \cos\Psi_S), \tag{2}$$

such that the current sheet is displaced to the south through amplitude $z_{N,S}$ when $\Psi_{N,S} = 0°$ modulo 360° and similarly to the north when $\Psi_{N,S} = 180°$ modulo 360°, with the two displacements thus adding when the two systems are in phase, and subtracting when they are in antiphase. Similarly, considering the thickness variations in Figure 2 we can write

$$D^*(\Psi_N,\ \Psi_S) = D - (D_N \cos\Psi_N - D_S \cos\Psi_S), \tag{3}$$

where D is the mean half-width of the current layer, such that the sheet is thickened by half-width D_N when $\Psi_N = 180°$ modulo 360° and by D_S when $\Psi_S = 0°$ modulo 360°, and correspondingly thinned by the same amounts when $\Psi_N = 0°$ modulo 360° and $\Psi_S = 180°$ modulo 360°, such that the two modulations add when the two PPO systems are in antiphase and subtract when they are in phase. We note that the modulation amplitudes must also satisfy $(D_N + D_S) < D$, such that D^* does not become unphysically zero or negative at any point during the PPO beat cycle. With regard to the relative amplitudes of the northern and southern modulations, we assume that the plasma sheet responds similarly to both northern and southern PPO systems, with modulation amplitudes that are approximately in proportion to the strength of the perturbation fields of the two PPO systems, whose north/south ratio k is shown in Figure 1c. This hypothesis implies in particular that when the two PPO systems are of near-equal amplitude, i.e., $k \approx 1$, a condition of particular relevance to the discussion by *Thomsen et al.* [2017] of the tail data during interval 2 in Figure 1, their effect on the plasma sheet will also be near equal, i.e., $(z_N/z_S) \approx (D_N/D_S) \approx 1$ in that case. This seems eminently reasonable since the northern and southern PPO systems are of entirely similar form as indicated in Figures 2a and 2c, such that there is no reason to suppose that the current/plasma sheet would respond differently to the two systems in that case. Adopting the simple wider hypothesis which includes this important special case, we then write

$$\left(\frac{z_N}{z_S}\right) \approx \left(\frac{D_N}{D_S}\right) \approx k, \tag{4}$$

as will be employed in the examples shown in section 4.

We now show that a characteristic feature of this system for phase differences away from either exactly in phase or antiphase as discussed above is that due to the differing behaviors of z^* and D^* with phases Ψ_N and Ψ_S, the current sheet has differing thicknesses when it is moving from south to north and from north to south, thus producing a sawtooth oscillatory field waveform that depends on the phase difference and relative amplitude of the two systems. Specifically, we consider the thickness of the current sheet at times

when the oscillating sheet passes through its mean position $z = 0$, moving both from south to north and from north to south. Taking the phase difference between the two systems (the "beat phase") to be $\Delta\Phi$ given by

$$\Delta\Phi = \Psi_N - \Psi_S, \tag{5}$$

substituting into equation (2) and setting $z^* = 0$ we find that the current sheet center passes through its mean position when

$$\tan\Psi_S = \frac{(1 + k\cos\Delta\Phi)}{k\sin\Delta\Phi}, \tag{6}$$

where we have chosen to express the result in terms of $\Delta\Phi$, near-constant during a given cycle, and the southern phase Ψ_S. We could equally have chosen to express the result in terms of $\Delta\Phi$ and the northern phase Ψ_N. For all values of $\Delta\Phi$ and k there exists two solutions of equation (6) for Ψ_S over the full modulo 360° range, separated by 180°, one corresponding to the south-to-north current sheet transition and the other to the north-to-south transition. Bearing in mind that the numerator and denominator in equation (6) can be taken either both positive or both negative for a given value of $\tan\Psi_S$, examination shows that the south-to-north transition takes place when

$$\sin\Psi_S = \frac{(1 + k\cos\Delta\Phi)}{\left(k^2 + 2k\cos\Delta\Phi + 1\right)^{1/2}} \quad \text{and} \quad \cos\Psi_S = \frac{k\sin\Delta\Phi}{\left(k^2 + 2k\cos\Delta\Phi + 1\right)^{1/2}}, \tag{7}$$

while the north-to-south transition takes place when

$$\sin\Psi_S = -\frac{(1 + k\cos\Delta\Phi)}{\left(k^2 + 2k\cos\Delta\Phi + 1\right)^{1/2}} \quad \text{and} \quad \cos\Psi_S = -\frac{k\sin\Delta\Phi}{\left(k^2 + 2k\cos\Delta\Phi + 1\right)^{1/2}}, \tag{8}$$

where the square root expression in the denominators is taken to be a positive quantity. Substituting equation (5) into equation (3) we can also write the modulation of the current sheet thickness using the same parameters as

$$D^* = D + D_S((1 - k\cos\Delta\Phi)\cos\Psi_S + k\sin\Delta\Phi\sin\Psi_S), \tag{9}$$

so that substituting from equation (7) for a south-to-north transition of the current layer we find

$$D^* = D + \frac{2kD_S\sin\Delta\Phi}{\left(k^2 + 2k\cos\Delta\Phi + 1\right)^{1/2}}, \tag{10a}$$

while substituting from equation (8) for a north-to-south transition of the current layer we similarly find

$$D^* = D - \frac{2kD_S\sin\Delta\Phi}{\left(k^2 + 2k\cos\Delta\Phi + 1\right)^{1/2}}. \tag{10b}$$

It can thus be seen from the $\sin\Delta\Phi$ factor in the numerators of equations (10a) and (10b) that if the northern oscillation leads the southern in phase, meaning that $0° < \Delta\Phi < 180°$ such that $\sin\Delta\Phi$ is positive, then the current sheet thickness is larger for south-to-north transitions ($D^* > D$ in equation (10a)) than it is for north-to-south transitions ($D^* < D$ in equation (10b)). Since, e.g., a south-to-north transition of the current sheet corresponds to the transition of a near-equatorial observer from the north tail to the south tail, it can be seen

that such a transition will take place more gradually (thicker current layer) than the subsequent transition back from the south tail to the north tail (thinner current layer), thus giving rise to a characteristic sawtooth oscillation of the B_r waveform. On the other hand, if the southern oscillation leads the northern in phase, meaning that $180° < \Delta\Phi < 360°$ (equivalent to $-180° < \Delta\Phi < 0°$ modulo 360°) so that $\sin\Delta\Phi$ is negative, then the current sheet thickness is larger for north-to-south transitions than it is for south-to-north transitions. In this case the south tail to north tail transitions of a near-equatorial observer will take place more gradually than the following north tail to south tail transitions, also leading to a sawtooth B_r waveform, but of opposite sense to that for $0° < \Delta\Phi < 180°$.

Due to the $\cos\Delta\Phi$ dependency of the denominators in equations (10a) and (10b), however, the largest such effects do not occur exactly at leading and lagging quadrature, i.e., at $\Delta\Phi = 90°$ and 270° where $\sin\Delta\Phi = \pm 1$, respectively, but at phases symmetrically closer to antiphase ($\Delta\Phi = 180°$) on either side. Differentiation of equation (10a) or (10b) shows that the maximum difference in thickness instead occurs at beat phases given for $k \leq 1$ by

$$\Delta\Phi = \cos^{-1}[-k], \tag{11a}$$

and for $k \geq 1$ by

$$\Delta\Phi = \cos^{-1}[-1/k], \tag{11b}$$

thus approaching antiphase on either side from quadrature as k approaches unity (equal amplitudes) from either zero (southern dominant) or infinity (northern dominant).

4. Illustrative Examples

We now illustrate this discussion with some examples calculated from equations (1a) and (1b) to (3). We use an undisturbed current sheet half-width $D = 2.5\ R_s$ consistent with the results of *Arridge et al*. [2011], and choose to examine the case of north/south amplitude ratio $k = 0.75$ for which beat effects between the two systems are very evident, but initially avoiding the special case of equal amplitudes, for which the model thickness modulations cancel out exactly when the two systems are in phase while the sheet displacements cancel out exactly when the two systems are in antiphase. We also choose a southern oscillation amplitude of $z_S = 4\ R_s$, thus with a northern amplitude of $z_N = 3\ R_S$ from equation (4), consistent with the results of *Arridge et al*. [2011] and *Szego et al*. [2012, 2013] for oscillations at radial distances of a few tens of R_s down-tail, such that the combined amplitude maximizes at 7 R_s when the two oscillations (and the two PPO systems) are in phase, but reduces to 1 R_s when they are in antiphase. Except near the latter condition, the overall oscillation amplitude will thus be comparable with the full 5 R_s width of the current sheet, exactly so when the two systems are in quadrature. The north-south motions will thus generally be sufficient to sweep the whole current sheet back and forth across a near-equatorial observer between the northern and southern outer plasma sheet or lobe, consistent with the general form of the B_r field modulations observed in the tail [*Jackman et al*., 2009; *Arridge et al*., 2011; *Provan et al*., 2012; *Szego et al*., 2012, 2013]. We further choose a southern current sheet thickness modulation amplitude of $D_S = 1\ R_s$, thus with a northern amplitude of $D_N = 0.75\ R_S$ from equation (4), such that the half-width of the current sheet given by equation (3) varies between limits of $D^* = 4.25\ R_s$ and 0.75 R_s when these oscillations are in phase with each other (when the two PPO systems are in antiphase) and between limits of $D^* = 2.75\ R_S$ and 2.25 R_s when these oscillations are in antiphase (when the two PPO systems are in phase). The results of *Provan et al*. [2012] are consistent with a strongly modulated half-width with peak values ~5 R_s when the two PPO systems are in antiphase, reducing to more weakly modulated half-widths of ~3 R_s when they are in phase (see their Figure 21), in approximate accord with these values.

Results are shown in Figures 3–6, where in each figure we fix the value of the beat phase $\Delta\Phi = \Psi_N - \Psi_S$, and plot current sheet parameters versus Ψ_S employed as a time proxy. For a fixed southern PPO period τ_S the southern phase at a given position (azimuth) increases linearly with time t as

$$\Psi_S = \Psi_{S\ 0} + \left(\frac{360\ \ t}{\tau_S}\right),$$

where Ψ_S is expressed in degrees and $\Psi_{S\ 0}$ is a constant. Figure 3 shows the case where the northern and

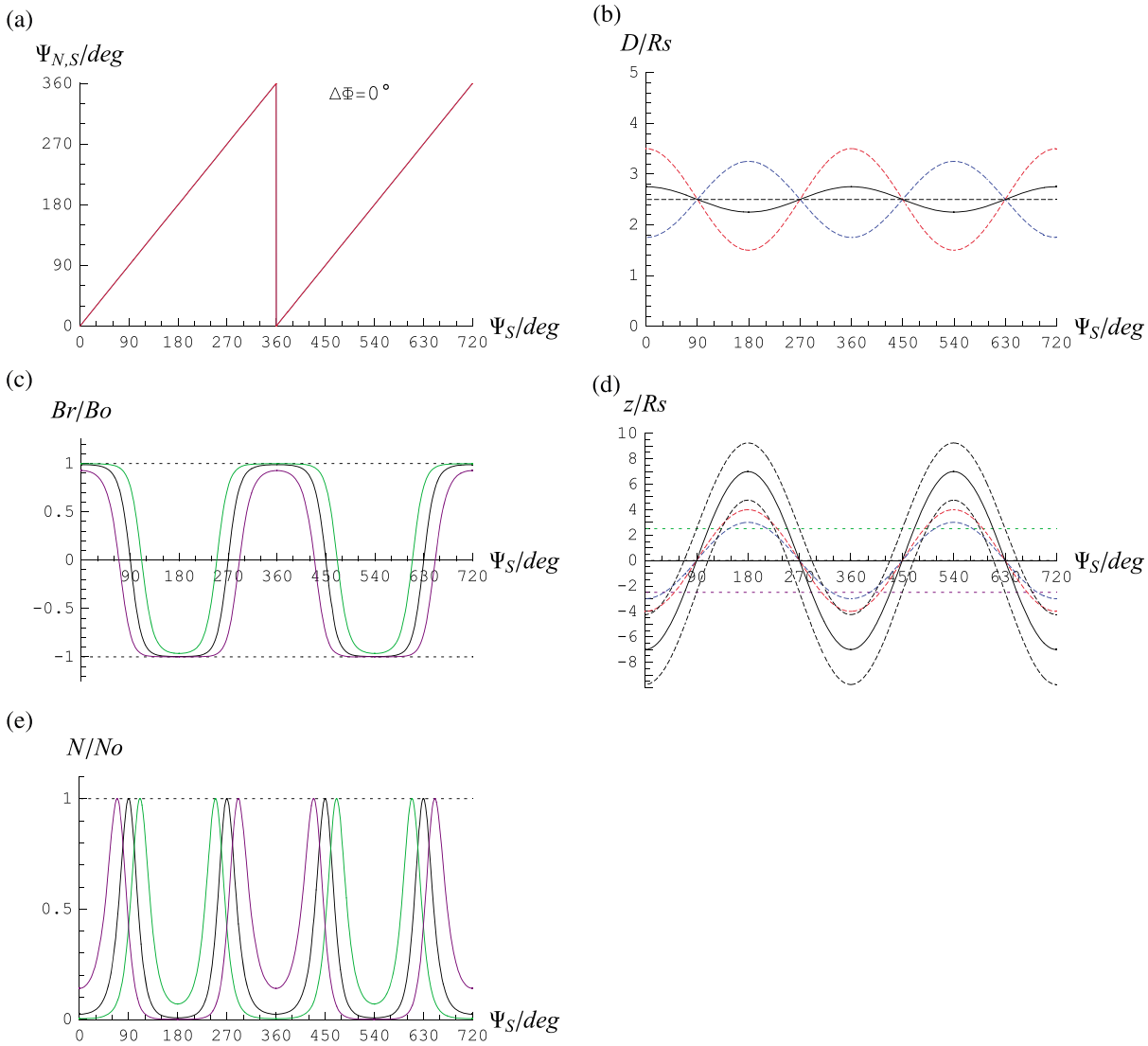

Figure 3. Plots showing the PPO-related modulations of the current sheet thickness and north-south position versus southern PPO phase Ψ_S employed as a time proxy, for the model in section 3 in the special case where the northern and southern PPO systems are in phase with each other, i.e., beat phase $\Delta\Phi = 0°$ modulo 360° (equation (5)). The model parameters are as given in section 4, namely, a southern north-south oscillation amplitude z_S of 4 R_s (about an undisturbed value of zero), a southern half-thickness modulation amplitude D_S of 1 R_s (about an undisturbed value of 2.5 R_s), together with northern modulations that are related to these by an assumed north/south amplitude ratio of $k = 0.75$. (a) The two phases $\Psi_{N,S}$ (deg), which are in this case equal (modulo 360°), over two cycles of oscillation. (b) The modulations of the sheet thickness (R_s) about the mean value of 2.5 R_s (horizontal black dashed line), where the blue and red dashed lines show the antiphase contributions of the individual northern and southern PPO systems, respectively, while the black line shows their sum (equation (3)), which nearly cancels in this case due to the $k = 0.75$ assumption. The red and blue dashed lines show (c) the in phase north-south displacements of the current sheet due to the individual northern and southern PPO systems, respectively, while the solid black line shows their sum (equation (2)). The black dashed lines on either side show the modulated northern and southern boundary regions of the current sheet, specifically $z^* \pm D^*$ from equations (2) and (3). (d) The modulations of the radial field component normalized to the lobe value, given by equation (1a). The black line corresponds to a fixed position at the mean position of the current sheet center $z = 0$, while the green and purple lines correspond to $z = \pm 2.5$ R_s near the undisturbed northern and southern boundaries of the current sheet, shown by the corresponding green and purple horizontal dotted lines in Figure 3c. We note that the related modulations of the B_θ field component are in phase with those of the sheet thickness D shown by the black line in Figure 3b. (e) The modulations of the plasma number density normalized to the value at the sheet center, given by equation (1b). The black, green, and purple lines correspond to the same z positions as in Figure 3d, indicated by the dotted lines in Figure 3c.

southern PPO systems are in phase with each other, $\Delta\Phi = 0°$ modulo 360°. Figure 3a shows the modulo 360° phase Ψ_S versus time (red line) over two full cycles, thus equal in this case to the northern phase Ψ_N modulo 360°. In this case the half-thickness modulations for the northern system shown in Figure 3b by the blue dashed line nearly cancel the modulations for the southern system shown by the red dashed line as given by equation (3), such that with $k = 0.75$ the remaining variations about the unperturbed half-thickness

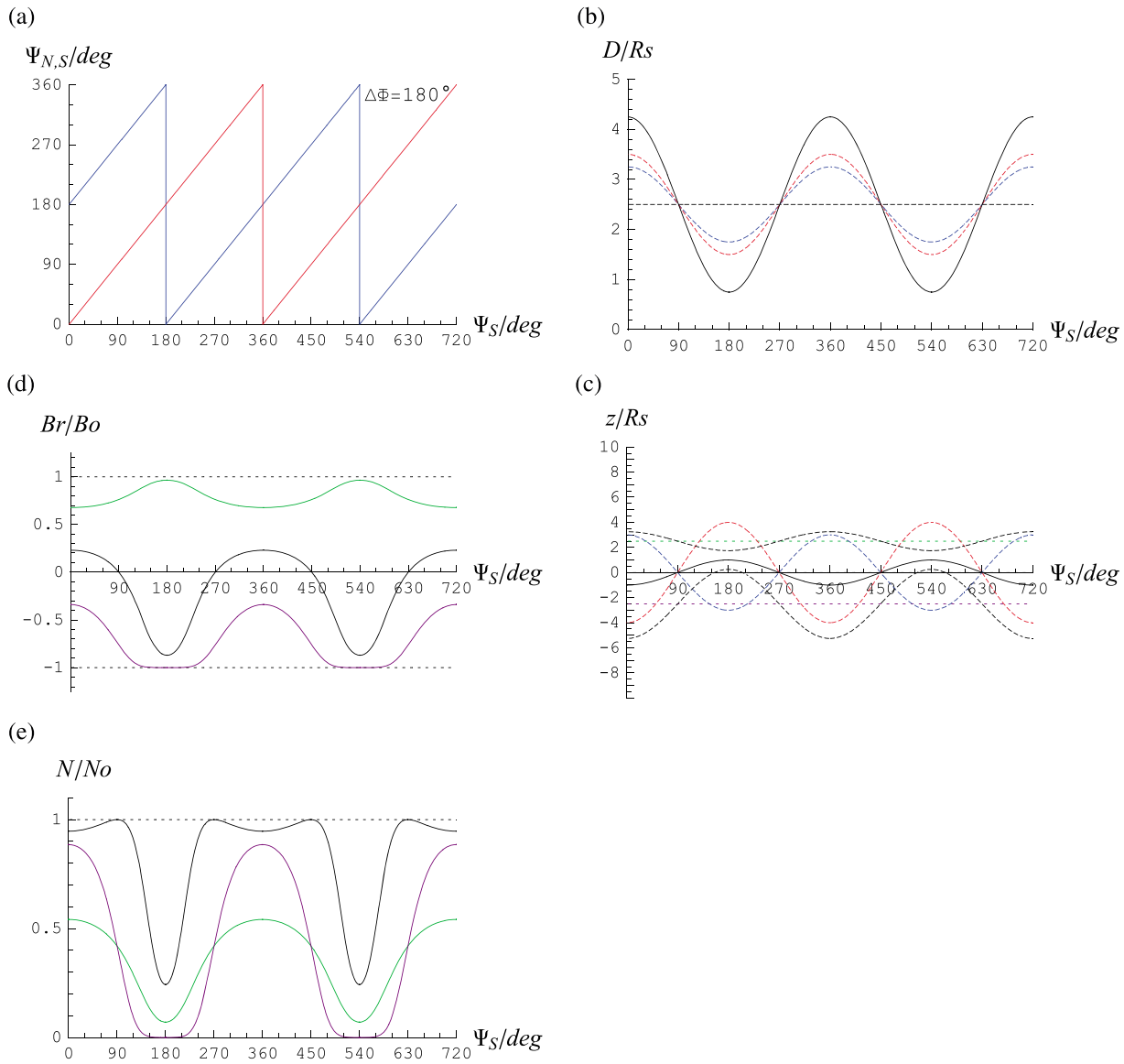

Figure 4. (a–e) Plots showing the PPO-related modulations of the current sheet thickness and position versus southern PPO phase Ψ_S for the model derived in section 3, using the same parameters as in Figure 3, i.e., $k = 0.75$, $z_S = 4\ R_s$, and $D_S = 1\ R_s$, but for the special case where the northern and southern PPO systems are in antiphase, $\Delta\Phi = 180°$ modulo 360°. The format is the same as Figure 3 except that in Figure 4a phase Ψ_S modulo 360° is shown by the red line exactly as in Figure 3a, while phase Ψ_N modulo 360° is shown by the blue line.

(horizontal black dashed line) have the same phase as the southern, but with a much reduced amplitude of 0.25 R_s (as indicated above), shown by the black solid line. However, the north-south oscillations of the sheet center shown by the blue and red dashed lines in Figure 3c, respectively, are in phase with each other, leading to a large combined north-south oscillation of the current sheet of amplitude 7 R_s, also shown by the black solid line (as also indicated above). The black dashed lines on either side indicate the width of the current sheet about its center position at any time (Ψ_S value), given by $z^* \pm D^*$ (equations (2) and (3)), which in this case is modulated to only a small extent about the mean value as indicated by Figure 3b, being slightly thicker when it is displaced to the south than when it is displaced to the north (as in Figure 2d). In Figure 3d we show the normalized radial component of the magnetic field versus time (Ψ_S value) given by equation (1a), determined at three fixed z positions relative to the mean position of the sheet center, namel,y the mean position of the sheet itself $z = 0$ (black line) and positions at $z = \pm 2.5\ R_s$ near the northern and southern boundaries of the undisturbed current sheet, shown by the green and purple lines, respectively. The latter

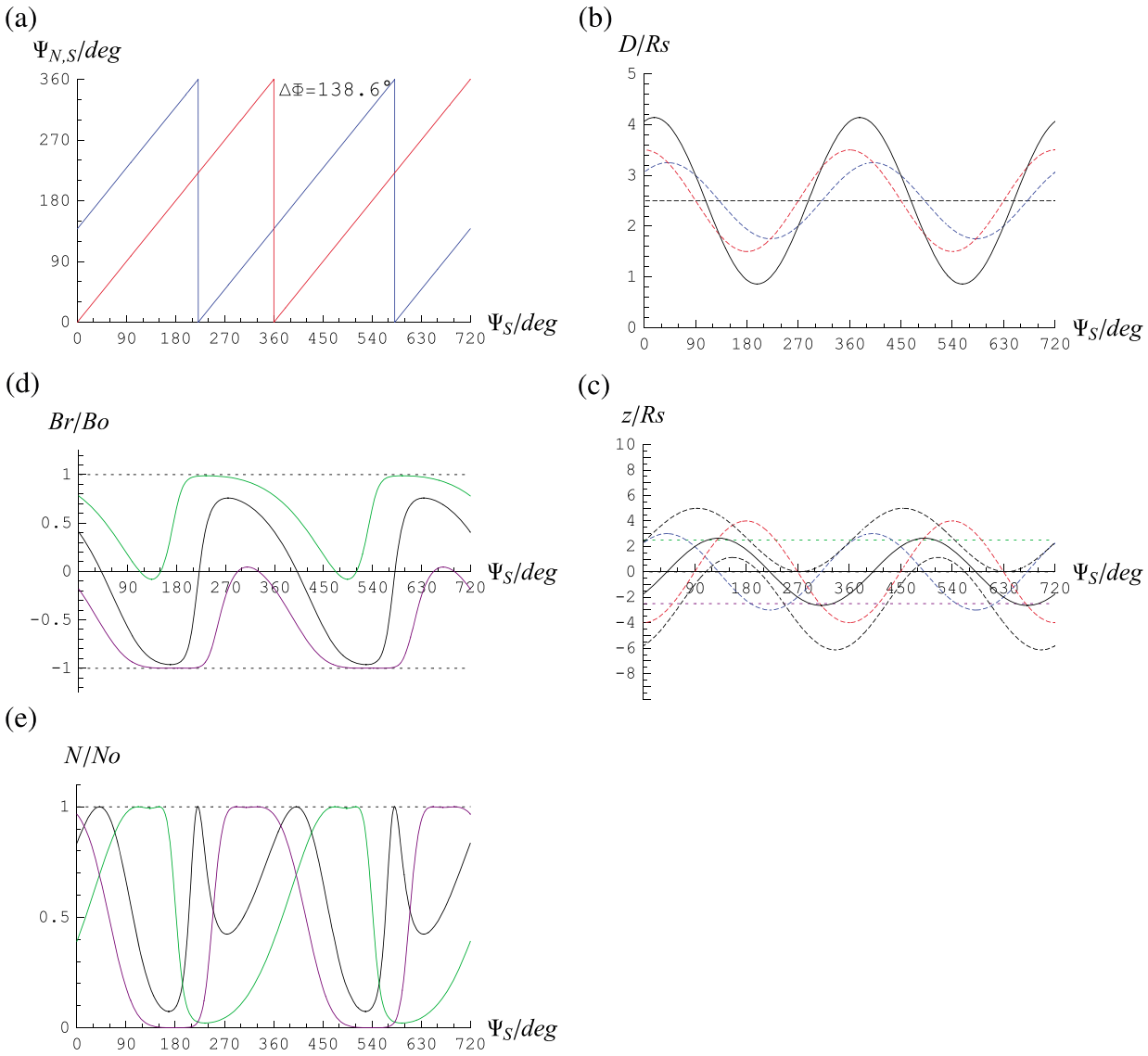

Figure 5. (a–e) Plots in the same format as Figures 3 and 4 showing the PPO-related modulations of the current sheet thickness and position versus southern PPO phase Ψ_S for the model derived in section 3, using the same parameters as in Figure 3, i.e., $k = 0.75$, $z_S = 4\ R_s$, and $D_S = 1\ R_s$, but for the case where the beat phase $\Delta\Phi = 138.59°$ modulo 360°, where the sawtooth effect maximizes in the range $0° < \Delta\Phi < 180°$.

positions are indicated in Figure 3c by the green and purple horizontal dotted lines. An observer at these locations will thus see transitions between the northern and southern outer plasma sheet and lobe that are symmetrical between north-to-south transitions that occur around $\Psi_S = 90°$ modulo 360°, and south-to-north transitions that occur around $\Psi_S = 270°$ modulo 360°. In addition, the profiles of the field variations in the northern hemisphere are almost mirror images of those occurring in the southern hemisphere, though not exactly so due to the small differences in current sheet thickness when its center lies in the northern and southern hemispheres. We also note in passing that the perturbations in the colatitudinal B_θ field threading the current sheet should approximately follow the form of the oscillations in the half-width D^* about the mean position D shown in Figure 3b, although the modulations in this specific case will be small. On the basis of the argument given in section 2, the current sheet is thinnest when B_θ is be smallest, and thickest when it is largest. Figure 3e shows the corresponding plasma number density normalized to the value at the sheet center versus time (Ψ_S value) given by equation (1b), plotted as black, green, and purple lines for the same three fixed z positions as in Figure 3d (see the similarly colored dashed lines in Figure 3c). Since the plasma sheet oscillation amplitude is large compared with the half thickness in this case, a sharp spike in density peaking at

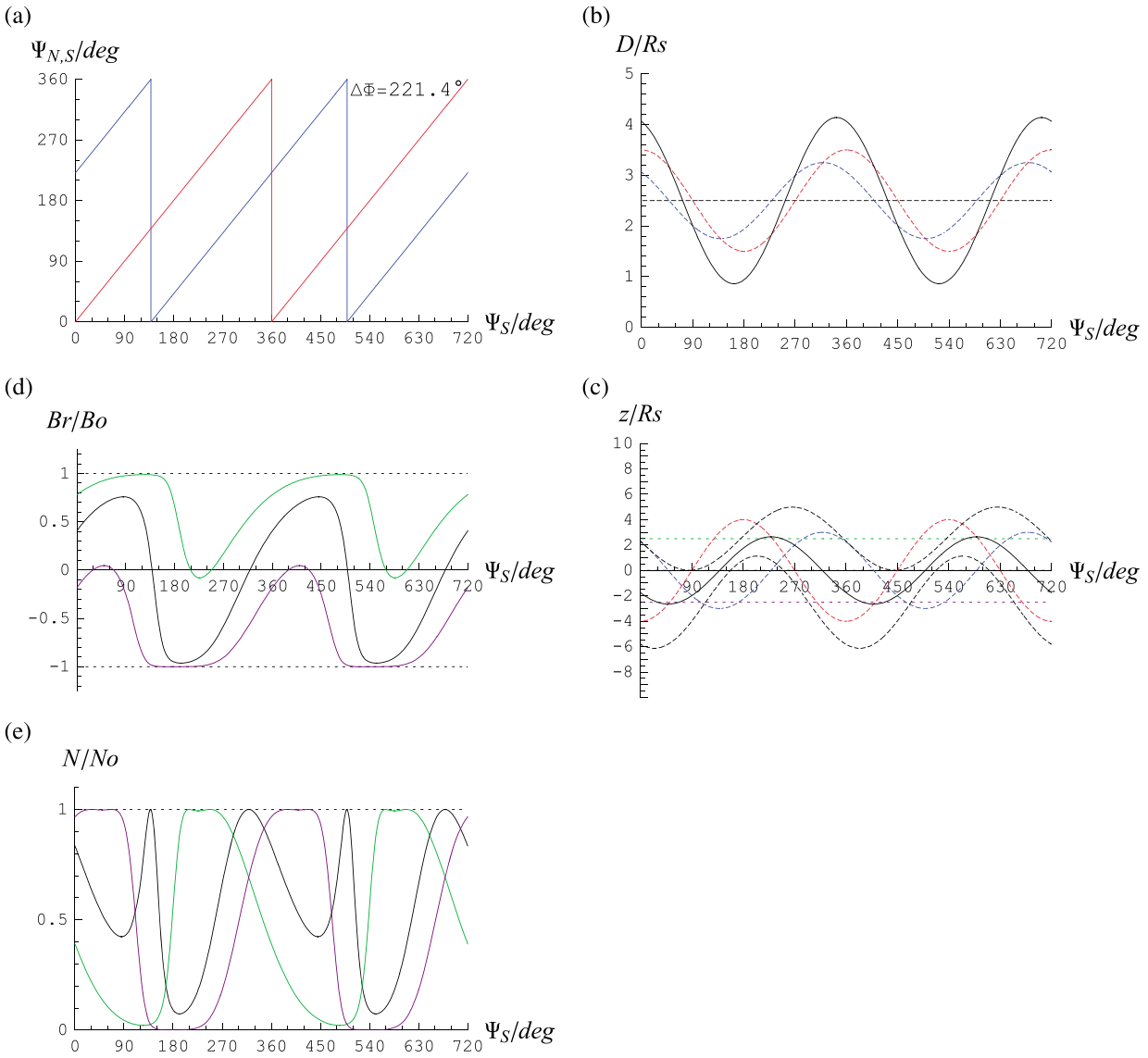

Figure 6. (a–e) Plots in the same format as Figures 3–5 showing the PPO-related modulations of the current sheet thickness and position versus southern PPO phase Ψ_S for the model derived in section 3, using the same parameters as in Figure 3, i.e., $k = 0.75$, $z_S = 4\ R_s$, and $D_S = 1\ R_s$, but for the case where the beat phase $\Delta\Phi = 221.41°$ modulo 360°, where the sawtooth effect maximizes in the range $180° < \Delta\Phi < 360°$, having the opposite sense of sawtooth effect for the range $0° < \Delta\Phi < 180°$ shown in Figure 5.

$N/N_o = 1$ occurs at the time when the center of the current sheet ($B_r/B_o = 0$) passes across the position in question, with the density then falling to small values in the northern and southern lobes on either side.

In Figure 4 we similarly show the opposite case in which the two PPO systems are in antiphase, $\Delta\Phi = 180°$. The format follows Figure 3, except that in Figure 4a the blue line now shows the northern phase $\Psi_N = \Psi_S \pm 180°$ modulo 360°, while the red line shows the southern phase Ψ_S modulo 360° exactly as in Figure 3a. In this case the current sheet half-thickness shown in Figure 4b is strongly modulated by the combined action of both the northern and southern PPO systems, with maximum and minimum values 4.25 and 0.75 R_s (as indicated above). Correspondingly, the north-south displacements due to the two systems shown in Figure 4c now nearly cancel, though with a small residual oscillation of amplitude 1 R_s with the same phasing as the southern oscillation due to the $k = 0.75$ assumption. The B_r/B_o variations at $z = 0$ in Figure 4d (black line) thus show corresponding transitions between the northern and southern current sheet, but these are very asymmetrical because the current sheet is much thinner when it is displaced to the north than when it is displaced to the south, giving larger negative fields in the former case than positive fields in the latter. The field perturbations

observed near the boundaries of the current sheet at $z = \pm 2.5\ R_s$ (green and purple lines) are dominated by the varying thickness of the current sheet rather than the residual positional oscillation, although the latter results in the two profiles not being quite mirror images of each other about $B_r/B_o = 0$. These field variations are reflected in the corresponding normalized plasma density variations shown in Figure 4e, which at $z = 0$ (black line) are very asymmetrical due to the thinness of the sheet when it is weakly displaced to the north, thus still producing a deep minimum in the density, followed by strongly increased thicknesses when it is weakly displaced to the south, resulting in an extended interval of elevated normalized densities near unity. As for the field variations in Figure 4d, the normalized density profiles on either side of the center (green and purple lines) are principally modulated by the variations in plasma sheet thickness, though not being symmetrical on either side due to the small residual north-south displacements.

We now show results for two intermediate cases, in which the northern phase leads the southern phase (i.e., $0° < \Delta\Phi < 180°$) in Figure 5, while the northern phase lags the southern phase (i.e., $180° < \Delta\Phi < 360°$, equivalent to $-180° < \Delta\Phi < 0°$ modulo 360°) in Figure 6. Rather than show simple quadrature, i.e., $\Delta\Phi = 90°$ and $\Delta\Phi = 270°$, however, we display the two phases for which the difference in sheet thickness for north to south and south to north transitions across $z = 0$ is maximum. From equation (11a) this condition occurs for $\Delta\Phi \approx 138.6°$ as shown in Figure 5, and at $\Delta\Phi \approx 221.4°$ as shown in Figure 6, phase angles that are thus displaced by ~41.4° on either side of antiphase. In both cases, the half-thickness oscillation amplitudes in Figures 5b and 6b are ~1.6 R_s, modestly reduced from the peak value of 1.75 R_s that occurs for the PPO antiphase condition shown in Figure 4b. Similarly, the north-south displacement amplitudes in Figures 5c and 6c are both ~2.6 R_s, roughly one third of the peak value of 7 R_s that occurs for the PPO in phase condition shown in Figure 3b. However, for $\Delta\Phi \approx 138.6°$, the combined half-thickness modulations are shifted to somewhat later phases in Figure 5b, while the combined north-south oscillations are shifted to significantly earlier phases in Figure 5c. For $\Delta\Phi \approx 221.4°$, the phase shifts are in the opposite sense, to earlier phases for the half-thickness in Figure 6b, and to later phases for the north-south displacement in Figure 6c. The net effect is that for $\Delta\Phi \approx 138.6°$ the half-thickness modulations are approximately in leading quadrature with the north-south displacement oscillations, such that the current sheet is thin when it is moving from north to south and thick when it is moving from south to north as can be seen in Figures 5b and 5c. Consequently, for a near-equatorial observer, the transitions from the north plasma sheet and lobe to the south take place more slowly than for the opposite transitions from the south plasma sheet and lobe to the north, giving rise to the characteristic sawtooth variations in B_r/B_o seen in Figure 5d. Correspondingly, the normalized plasma density in Figure 5e (black line) remains elevated about the peak value at the sheet center for a longer interval in the transitions from the north plasma sheet and lobe to the south, than in the transitions from the south plasma sheet and lobe to the north. The opposite phase shifts that occur for $\Delta\Phi \approx 221.4°$ in Figure 6 result in the half-thickness modulations being approximately in lagging quadrature with the north-south displacement oscillations, such that the current sheet is thin when it is moving from south to north and thick when it is moving from north to south as seen in Figures 6b and 6c. Consequently, for a near-equatorial observer in this case, the transitions from the south plasma sheet and lobe to the north take place more slowly than for the opposite transitions from the north plasma sheet and lobe to the south, also giving rise to a characteristic sawtooth variation in B_r/B_o shown in Figure 6d, but now having the opposite sense to that in Figure 5d. The corresponding variations in the normalized plasma density in Figure 6e (black line) similarly show opposite asymmetries to those in Figure 5e. We note that according to the discussion in sections 2 and 3, B_θ should be elevated during the slower transitions (thicker current sheet) and diminished during the subsequent faster transitions (thinner current sheet).

In principle, the same sheet thickness asymmetries between north-to-south and south-to-north transitions exist over the whole range of $\Delta\Phi$ values except for exactly in phase and antiphase conditions shown in Figures 3 and 4, thus leading to sawtooth asymmetries in the field profiles. However, examination shows that these effects remain relatively weak over a range of $\Delta\Phi$ values of several tens of degrees centered on in phase conditions $\Delta\Phi = 0°$, while remaining evident to within ~10° of antiphase $\Delta\Phi = 180°$ for this value of k. This is illustrated in Figure 7, where we show B_r/B_o profiles in the same format as Figures 3d–6d for pairs of $\Delta\Phi$ values spaced equally on either side of PPO antiphase (and hence also PPO in phase) conditions. Specifically, Figures 7a and 7b show profiles for $\Delta\Phi = 45°$ and 315°, respectively, which remain similar to the PPO in phase profiles in Figure 3d, although opposite slight asymmetries are evident in the north-to-south and south-to-north transitions in the two cases. These asymmetries become more clearly marked for

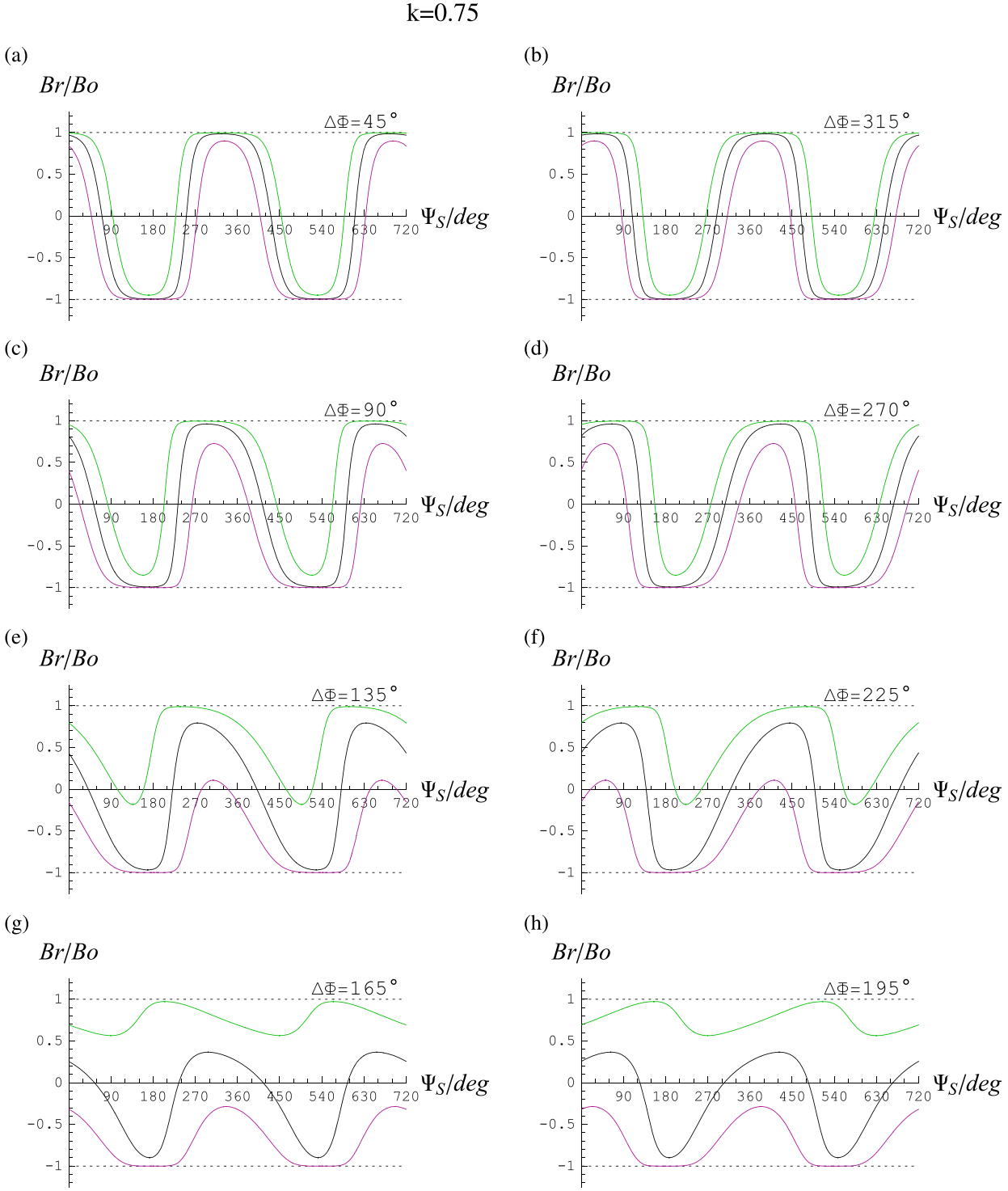

Figure 7. Set of plots of the radial field component normalized to the lobe value versus southern PPO phase Ψ_S, in the same format as Figures 3d–6d. We use the same model parameters as for Figures 3–6, i.e., $k = 0.75$, $z_S = 4$ R_s, and $D_S = 1$ R_s, but now with beat phases $\Delta\Phi$ equal to (a) 45°, (b) 315°, (c) 90°, (d) 270°, (e) 135°, (f) 225°, (g) 165°, and (h) 195°, such that horizontal plot pairs, Figures 7a and 7b and Figures 7c and 7d, and so on, show conditions separated equally in phase on either side of antiphase.

PPO quadrature conditions $\Delta\Phi = 90°$ and 270° shown in Figures 7c and 7d, respectively, and even more so for $\Delta\Phi = 135°$ and 225° shown in Figures 7e and 7f, respectively, representing conditions $\pm 45°$ on either side of PPO antiphase close to the cases for maximum opposite sawtooth effects shown in Figures 5 and 6. In

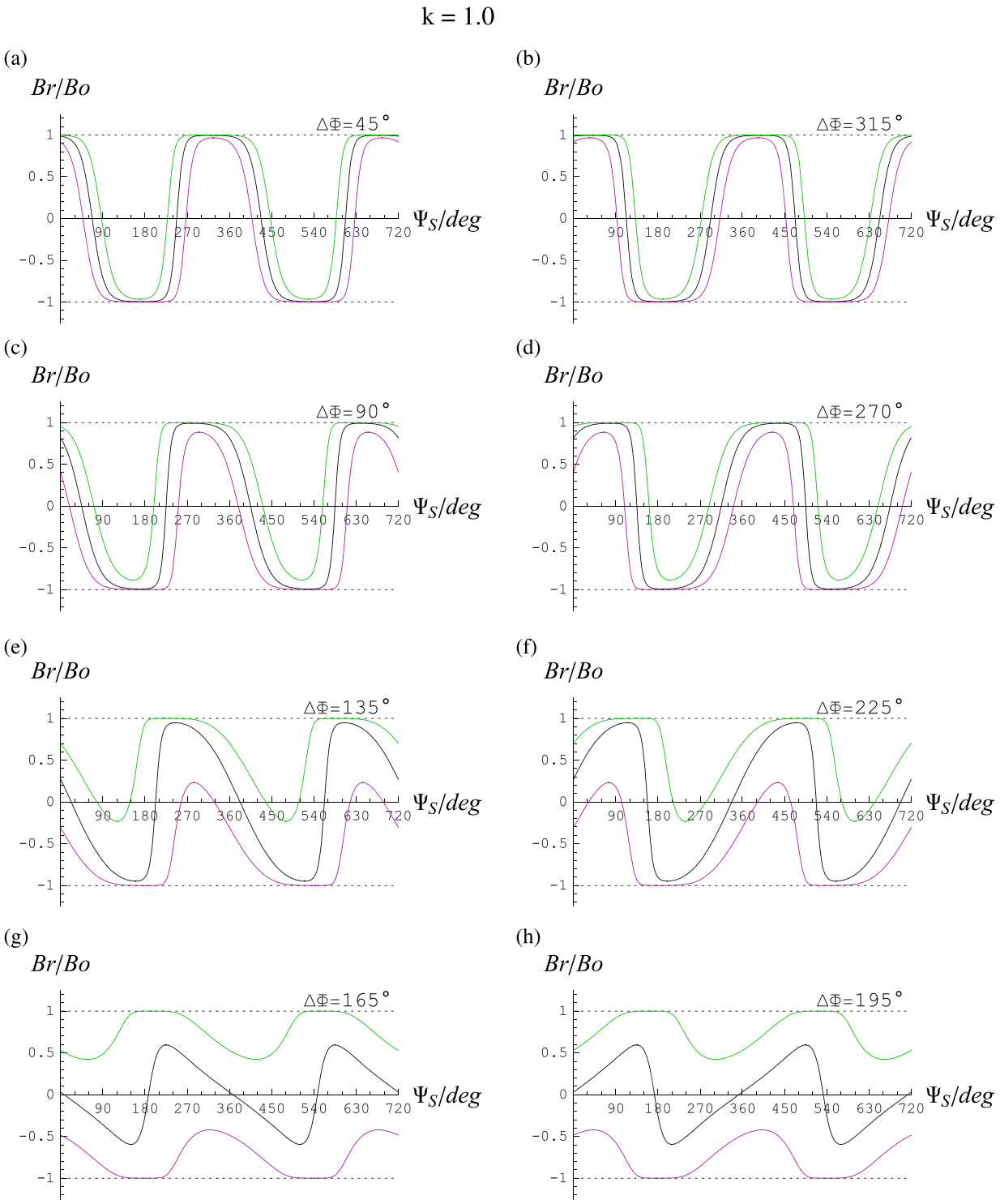

Figure 8. (a–h) Set of plots of the radial field component normalized to the lobe value versus southern PPO phase Ψ_S, in the same format as Figure 7 but for model parameters $k = 1.0$, $z_S = z_N = 4\ R_s$, and $D_S = D_N = 1\ R_s$. The beat phase values shown in each panel are the same as in Figure 7.

Figures 7g and 7h for $\Delta\Phi = 165°$ and 195°, respectively, the profiles now approach those shown for antiphase $\Delta\Phi = 180°$ in Figure 4d, but the sawtooth asymmetry is still quite evident at near-equatorial locations.

We now briefly explore the effect of varying the north/south amplitude ratio k, examining in particular values that are appropriate to differing intervals of Cassini observations as shown in Figure 1. In Figure 8 we show

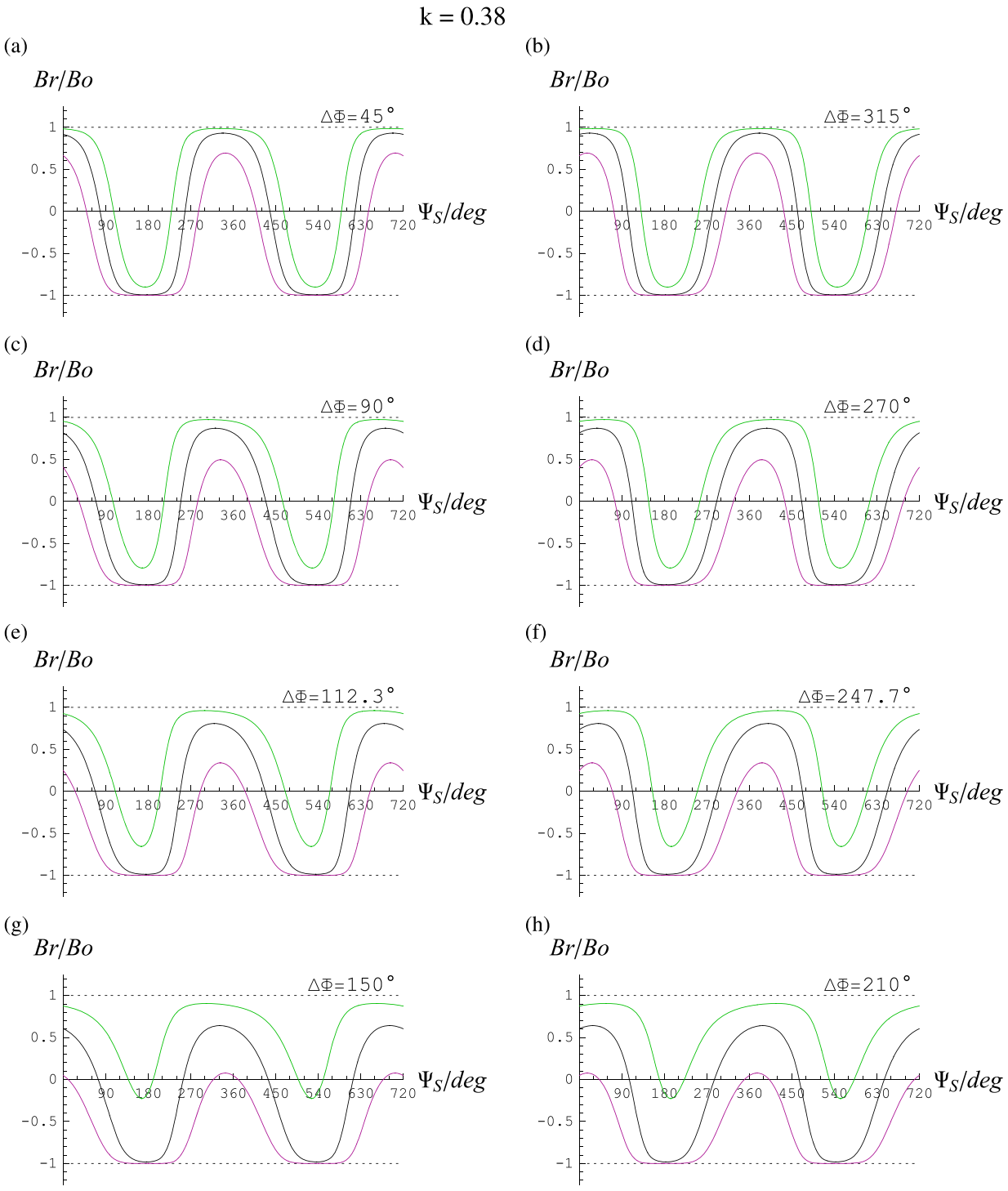

Figure 9. Set of plots of the radial field component normalized to the lobe value versus southern PPO phase Ψ_S, in the same format as Figures 7 and 8 but for model parameters $k = 0.38$, $z_S = 4$ R_s, and $D_S = 1$ R_s, and with beat phases $\Delta\Phi$ equal to (a) 45°, (b) 315°, (c) 90°, (d) 270°, (e) 112.334°, (f) 247.666°, (g) 150°, and (h) 210°, where the phase differences shown in Figures 9e and 9f correspond to conditions of maximum sawtooth effect of opposite senses for this value of k (equation (11a)).

results for equal amplitudes of the northern and southern systems $k = 1$, as applies, e.g., to near-equinoctial conditions during the 2009–2010 season of tail observations (interval 2 in Figure 1), for which sawtooth asymmetry effects are maximal. We choose the same southern modulation amplitudes as in Figures 3-6, such that $z_S = z_N = 4$ R_s and $D_S = D_N = 1$ R_s, and in Figures 8a–8h show exactly the same phase difference values as in

Figures 6a–6h, so that the results in the two figures can be compared directly. The asymmetry effects are seen to be comparable in the two cases, but generally more marked for $k = 1$ than for $k = 0.75$, and now with strict symmetry between observation points at equal distances on either side of the current sheet (green and purple profiles). The sawtooth effects for near-equatorial observing points approaching antiphase conditions in Figures 8g and 8h are particularly striking. Overall, these results provide a reasonable explanation of the findings of *Thomsen et al.* [2017] for the 2010 tail data.

In Figure 9 we show results in the same format for $k = 0.38$, taken together with $z_S = 4\ R_s$ and $D_S = 1\ R_s$, corresponding to southern summer conditions during the 2006 season of tail observations (interval 1 in Figure 1). The PPO phase difference angles in Figures 9a–9d are the same as those in Figures 7a–7d and 8a–8d, respectively, while in Figures 9e and 9f we show conditions of maximum opposite sawtooth asymmetry effects for this value of k given by equation (11a), i.e., $\Delta\Phi \approx 112.3°$ and $\Delta\Phi \approx 247.7°$, and in Figures 9g and 9h we show results for $\Delta\Phi = 150°$ and $\Delta\Phi = 210°$, respectively, approaching antiphase. While sawtooth asymmetry effects are still evident in these cases, the effect is considerably muted compared with that displayed in Figures 7 and 8 and would likely be difficult to discern even at their maximum (Figures 9e and 9f) in the presence of other significant sources of tail field variability. Instead, the main PPO effects evident in this case are just those related to the north-south displacements and thickening and thinning effects due to the dominant southern PPO system. However, the northern PPO system contributes to maximum displacement amplitudes with minimum thickness modulations for near-in phase conditions around $\Delta\Phi = 0°$, as seen in Figures 9a and 9b, and minimum displacement amplitudes with maximum thickness modulations for near-antiphase conditions around $\Delta\Phi = 180°$, as seen in Figures 9g and 9h. Given these results it seems unsurprising that sawtooth effects in the tail field were not obvious during the 2006 interval of tail observations [*Thomsen et al.*, 2017].

We have also examined northern-dominant $k = 2.3$ conditions (i.e., $1/k \approx 0.44$), together with $z_N = 4\ R_s$ and $D_N = 1\ R_s$, which applies to postperiod reversal northern spring conditions in early 2015 (the first part of interval 3 in Figure 1). Unsurprisingly, the results are similar to those for $k = 0.38$ in Figure 9, showing slightly stronger but still relatively weak asymmetries due to the effect of the weaker southern PPO system on the dominant northern PPO modulations, and are not therefore reproduced here. Overall, examination shows that for the empirically determined modulation amplitudes employed here, maximum sawtooth asymmetries for relative phases near those given by equations (11a) or (11b) only become quite clearly evident for cases in which the amplitude of one PPO system does not exceed twice that of the other, i.e., roughly for north/south amplitude ratios k in the range $0.5 < k < 2$.

5. Summary

We have considered the modulation effects on Saturn's equatorial magnetotail and magnetodisk current sheet produced by the magnetic perturbations associated with the ubiquitous PPOs, focusing on the effects due to the northern and southern systems combined. Previous studies have noted that the current sheet will be displaced to the south for positive radial perturbation fields and to the north for negative radial perturbation fields, and that it will be thickened for positive colatitudinal perturbation fields (in the same sense as the planetary field) and thinned for negative colatitudinal perturbation fields [*Andrews et al.*, 2010a; *Provan et al.*, 2012; *Jackman et al.*, 2016]. However, the relative phasing of the radial and colatitudinal perturbation fields is opposite for the two PPO systems, in phase for the southern system and antiphase for the northern system, such that for the southern system the current sheet is thickened when it is displaced to the south at southern PPO phase $\Psi_S = 0°$ and thinned when it is displaced to the north at phase $\Psi_S = 180°$, while for the northern system the current sheet is thinned when it is displaced to the south at northern PPO phase $\Psi_N = 0°$ and thickened when it is displaced to the north at phase $\Psi_N = 180°$. These are the principal effects observed under conditions in which one of these PPO systems dominates the modulations, as was the case for the southern system during postsolstice southern summer conditions early in the Cassini mission (north/south ratio of ~0.4 during ~2005–2007).

During near-equinoctial conditions (~2008–2010), however, the amplitudes of the two systems became near equal, such that we must then consider their combined effect, depending on the relative phases of the two systems, $\Delta\Phi = \Psi_N - \Psi_S$. It is evident that when the two systems are in phase, $\Delta\Phi = 0°$ modulo 360°, the north-south oscillations of the sheet due to the two systems will reinforce each other, while the thickening and thinning will tend to cancel, while when the two systems are in antiphase, $\Delta\Phi = 180°$ modulo 360°, the thickening

and thinning modulations of the sheet due to the two systems will reinforce each other, while the north-south oscillations will tend to cancel [*Provan et al*., 2012; *Jia and Kivelson*, 2012; *Jackman et al*., 2016]. Here we have also for the first time investigated intermediate relative phases of the two systems and have shown that their opposite phase behaviors result in sawtooth modulations of the principal radial field in the tail. Specifically, when the phase of the northern system leads that of the southern, i.e., $0° < \Delta\Phi < 180°$, the current sheet is thicker when moving from south to north than when moving from north to south. Consequently, for a near-equatorial observer the transitions from the north to the south tail due to the south-to-north motion take place more slowly than the subsequent transitions from the south to the north tail due to the north-to-south motion, such that the observed variation in the radial field has a sawtooth waveform. When the phase of the northern system lags that of the southern system, however, i.e., $180° < \Delta\Phi < 360°$, equivalent to $-180° < \Delta\Phi < 0°$ modulo 360°, the current sheet is thicker when moving from north to south than when moving from south to north. Consequently, for a near-equatorial observer the transitions from the south to the north tail due to the north-to-south motion take place more slowly than the subsequent transitions from the north to the south tail due to the south-to-north motion, such that the variation in the radial field again has a sawtooth waveform but of the opposite sense to that occurring when the phase of the northern system leads that of the southern. Corresponding asymmetries also occur in the normalized plasma density profiles between the transitions from the north to the south tail and from the south to the north tail, as may then be expected.

For a given value of the north/south PPO amplitude ratio k the maximum sawtooth effect occurs at a relative phase $\Delta\Phi$ that lies near quadrature, i.e., $\Delta\Phi = 90°$ and 270°, when one PPO system dominates the other, i.e., for $k \to 0$ or $k \to \infty$, and moves symmetrically toward antiphase $\Delta\Phi = 180°$ on either side for near-equal amplitudes, i.e., for $k \to 1$ (see equations (11a) and (11b)). Given empirically determined amplitudes of typically ~4 R_s for the north-south oscillations and ~1 R_s for the thickness, however, the maximum sawtooth effect on the radial field profiles is found to be small when one system dominates the other, and only becomes an obvious effect when the two amplitudes become comparable, roughly when the amplitude of one system lies within a factor of 2 of the other, i.e., for k in the range $0.5 < k < 2$. We thus suggest that these results provide a simple basis on which to understand the observational findings presented by *Thomsen et al*. [2017].

Acknowledgments
Work at the University of Leicester was supported by STFC consolidated grant ST/N000749/1. G.J.H. was supported by STFC Quota Studentship ST/K502121/1. C.M.J. was supported by STFC Ernest Rutherford Fellowship number ST/L004399/1. This paper is theoretical in nature and employs no data other than those in the references cited.

References

Andrews, D. J., E. J. Bunce, S. W. H. Cowley, M. K. Dougherty, G. Provan, and D. J. Southwood (2008), Planetary period oscillations in Saturn's magnetosphere: Phase relation of equatorial magnetic field oscillations and SKR modulation, *J. Geophys. Res.*, *113*, A09205, doi:10.1029/2007JA012937.

Andrews, D. J., S. W. H. Cowley, M. K. Dougherty, and G. Provan (2010a), Magnetic field oscillations near the planetary period in Saturn's equatorial magnetosphere: Variation of amplitude and phase with radial distance and local time, *J. Geophys. Res.*, *115*, A04212, doi:10.1029/2009JA0014729.

Andrews, D. J., A. J. Coates, S. W. H. Cowley, M. K. Dougherty, L. Lamy, G. Provan, and P. Zarka (2010b), Magnetospheric period oscillations at Saturn: Comparison of equatorial and high-latitude magnetic field periods with north and south SKR periods, *J. Geophys. Res.*, *115*, A12252, doi:10.1029/2010JA015666.

Andrews, D. J., S. W. H. Cowley, M. K. Dougherty, L. Lamy, G. Provan, and D. J. Southwood (2012), Planetary period oscillations in Saturn's magnetosphere: Evolution of magnetic oscillation properties from southern summer to post-equinox, *J. Geophys. Res.*, *117*, A04224, doi:10.1029/2011JA017444.

Arridge, C. S., K. K. Khurana, C. T. Russell, D. J. Southwood, N. Achilleos, M. K. Dougherty, A. J. Coates, and H. K. Leinweber (2008), Warping of Saturn's magnetospheric and magnetotail current sheets, *J. Geophys. Res.*, *113*, A08217, doi:10.1029/2007JA012963.

Arridge, C. S., et al. (2011), Periodic motion of Saturn's nightside plasma sheet, *J. Geophys. Res.*, *116*, A11205, doi:10.1029/2011JA016827.

Burch, J. L., A. D. DeJong, J. Goldstein, and D. T. Young (2009), Periodicity in Saturn's magnetosphere: Plasma cam, *Geophys. Res. Lett.*, *36*, L14203, doi:10.1029/2009GL039043.

Burton, M. E., M. K. Dougherty, and C. T. Russell (2010), Saturn's internal planetary magnetic field, *Geophys. Res. Lett.*, *37*, L24105, doi:10.1029/2010GL045148.

Carbary, J. F., and S. M. Krimigis (1982), Charged particle periodicity in the Saturnian magnetosphere, *Geophys. Res. Lett.*, *9*, 1073–1076, doi:10.1029/GL009i009p01073.

Carbary, J. F., D. G. Mitchell, S. M. Krimigis, and N. Krupp (2007), Electron periodicities in Saturn's outer magnetosphere, *J. Geophys. Res.*, *112*, A03206, doi:10.1029/2006JA012077.

Carbary, J. F., D. G. Mitchell, P. Brandt, C. Paranicas, and S. M. Krimigis (2008a), ENA periodicities at Saturn, *Geophys. Res. Lett.*, *35*, L07102, doi:10.1029/2008GL033230.

Carbary, J. F., D. G. Mitchell, P. Brandt, E. C. Roelof, and S. M. Krimigis (2008b), Periodic tilting of Saturn's plasma sheet, *Geophys. Res. Lett.*, *35*, L24101, doi:10.1029/2008GL036339.

Cowley, S. W. H., and G. Provan (2015), Planetary period oscillations in Saturn's magnetosphere: Comments on the relation between post-equinox periods determined from magnetic field and SKR emission data, *Ann. Geophys.*, *33*, 901–912, doi:10.5194/angeo-33-901-2015.

Cowley, S. W. H., and G. Provan (2016), Planetary period oscillations in Saturn's magnetosphere: Further comments on the relationship between post-equinox properties deduced from magnetic field and Saturn kilometric radiation measurements, *Icarus*, *272*, 258–276, doi:10.1016/j.icarus.2016.02.051.

Cowley, S. W. H., D. M. Wright, E. J. Bunce, A. C. Carter, M. K. Dougherty, G. Giampieri, J. D. Nichols, and T. R. Robinson (2006), Cassini observations of planetary-period magnetic field oscillations in Saturn's magnetosphere: Doppler shifts and phase motion, *Geophys. Res. Lett.*, *33*, L07104, doi:10.1029/2005GL025522.

Cowley, S. W. H., P. Zarka, G. Provan, L. Lamy, and D. J. Andrews (2016), Comment on "A new approach to Saturn's periodicities" by J. F. Carbary, *J. Geophys. Res. Space Physics*, *121*, 2418–2422, doi:10.1002/2015JA021996.

Desch, M. D., and M. L. Kaiser (1981), Voyager measurement of the rotation period of Saturn's magnetic field, *Geophys. Res. Lett.*, *8*, 253–256, doi:10.1029/GL008i003p00253.

Espinosa, S. A., and M. K. Dougherty (2000), Periodic perturbations in Saturn's magnetic field, *Geophys. Res. Lett.*, *27*, 2785–2788, doi:10.1029/2000GL000048.

Galopeau, P. H. M., and A. Lecacheux (2000), Variations of Saturn's radio rotation period measured at kilometer wavelengths, *J. Geophys. Res.*, *105*, 13,089–13,101, doi:10.1029/1999JA005089.

Gurnett, D. A., et al. (2005), Radio and plasma wave observations at Saturn from Cassini's approach and first orbit, *Science*, *307*, 1255–1259, doi:10.1126/science.1105356.

Gurnett, D. A., A. Lecacheux, W. S. Kurth, A. M. Persoon, J. B. Groene, L. Lamy, P. Zarka, and J. F. Carbary (2009a), Discovery of a north-south asymmetry in Saturn's radio rotation period, *Geophys. Res. Lett.*, *36*, L16102, doi:10.1029/2009GL039621.

Gurnett, D. A., A. M. Persoon, J. B. Groene, A. J. Kopf, G. B. Hospodarsky, and W. S. Kurth (2009b), A north-south difference in the rotation rate of auroral hiss at Saturn: Comparison to Saturn's kilometric radio emission, *Geophys. Res. Lett.*, *36*, L21108, doi:10.1029/2009GL040774.

Gurnett, D. A., J. B. Groene, A. M. Persoon, J. D. Menietti, S.-Y. Ye, W. S. Kurth, R. J. MacDowell, and A. Lecacheux (2010), The reversal of the rotational modulation rates of the north and south components of Saturn kilometric radiation near equinox, *Geophys. Res. Lett.*, *37*, L24101, doi:10.1029/2010GL045796.

Gurnett, D. A., J. B. Groene, T. F. Averkamp, W. S. Kurth, S.-Y. Ye, and G. Fischer (2011), The SLS4 longitude system based on a tracking filter analysis of the rotational modulation of Saturn kilometric radiation, in *Planetary Radio Emissions VII*, edited by H. O. Rucker, et al., pp. 51–64, Austrian Acad. Sci. Press, Vienna.

Hunt, G. J., S. W. H. Cowley, G. Provan, E. J. Bunce, I. I. Alexeev, E. S. Belenkaya, V. V. Kalegaev, M. K. Dougherty, and A. J. Coates (2015), Field-aligned currents in Saturn's northern nightside magnetosphere: Evidence for inter-hemispheric current flow associated with planetary period oscillations, *J. Geophys. Res. Space Physics*, *120*, 7552–7584, doi:10.1002/2015JA021454.

Jackman, C. M., C. S. Arridge, H. J. McAndrews, M. G. Henderson, and R. J. Wilson (2009), Northward field excursions in Saturn's magnetotail and their relationship to magnetospheric periodicities, *Geophys. Res. Lett.*, *36*, L16101, doi:10.1029/2009GL039149.

Jackman, C. M., G. Provan, and S. W. H. Cowley (2016), Reconnection events in Saturn's magnetotail: Dependence of plasmoid occurrence on planetary period oscillation phase, *J. Geophys. Res. Space Physics*, *121*, 2922–2934, doi:10.1002/2015JA021985.

Jia, X., and M. G. Kivelson (2012), Driving Saturn's magnetospheric periodicities from the upper atmosphere/ionosphere: Magnetotail response to dual sources, *J. Geophys. Res.*, *117*, A11219, doi:10.1029/2012JA018183.

Kurth, W. S., T. F. Averkamp, D. A. Gurnett, J. B. Groene, and A. Lecacheux (2008), An update to a Saturnian longitude system based on kilometric radio emissions, *J. Geophys. Res.*, *113*, A05222, doi:10.1029/2007JA012861.

Lamy, L. (2011), Variability of southern and northern SKR periodicities, in *Planetary Radio Emissions VII*, edited by H. O. Rucker et al., pp. 39–50, Austrian Acad. Sci. Press, Vienna.

Morooka, M. W., et al. (2009), The electron density of Saturn's magnetosphere, *Ann. Geophys.*, *27*, 2971–2991, doi:10.5194/angeo-27-2971-2009.

Nichols, J. D., J. T. Clarke, S. W. H. Cowley, J. Duval, A. J. Farmer, J.-C. Gérard, D. Grodent, and S. Wannawichian (2008), Oscillation of Saturn's southern auroral oval, *J. Geophys. Res.*, *113*, A11205, doi:10.1029/2008JA013444.

Nichols, J. D., B. Cecconi, J. T. Clarke, S. W. H. Cowley, J.- C. Gérard, A. Grocott, D. Grodent, L. Lamy, and P. Zarka (2010a), Variation of Saturn's UV aurora with SKR phase, *Geophys. Res. Lett.*, *37*, L15102, doi:10.1029/2010GL044057.

Nichols, J. D., S. W. H. Cowley, and L. Lamy (2010b), Dawn-dusk oscillation of Saturn's conjugate auroral ovals, *Geophys. Res. Lett.*, *37*, L24102, doi:10.1029/2010GL045818.

Provan, G., D. J. Andrews, C. S. Arridge, S. W. H. Cowley, S. E. Milan, M. K. Dougherty, and D. M. Wright (2009), Polarization and phase of planetary period oscillations on high latitude field lines in Saturn's magnetosphere, *J. Geophys. Res.*, *114*, A02225, doi:10.1029/2008JA013782.

Provan, G., D. J. Andrews, B. Cecconi, S. W. H. Cowley, M. K. Dougherty, L. Lamy, and P. Zarka (2011), Magnetospheric period magnetic field oscillations at Saturn: Equatorial phase 'jitter' produced by superposition of southern- and northern-period oscillations, *J. Geophys. Res.*, *116*, A04225, doi:10.1029/2010JA016213.

Provan, G., D. J. Andrews, C. S. Arridge, A. J. Coates, S. W. H. Cowley, G. Cox, M. K. Dougherty, and C. M. Jackman (2012), Dual periodicities in planetary-period magnetic field oscillations in Saturn's tail, *J. Geophys. Res.*, *117*, A01209, doi:10.1029/2011JA017104.

Provan, G., S. W. H. Cowley, J. Sandhu, D. J. Andrews, and M. K. Dougherty (2013), Planetary period magnetic field oscillations in Saturn's magnetosphere: Post-equinox abrupt non-monotonic transitions to northern system dominance, *J. Geophys. Res. Space Physics*, *118*, 3243–3264, doi:10.1002/jgra.50186.

Provan, G., L. Lamy, S. W. H. Cowley, and M. K. Dougherty (2014), Planetary period oscillations in Saturn's magnetosphere: Comparison of magnetic oscillations and SKR modulations in the post-equinox interval, *J. Geophys. Res. Space Physics*, *119*, 7380–7401, doi:10.1002/2014JA020011.

Provan, G., S. W. H. Cowley, L. Lamy, E. J. Bunce, G. J. Hunt, P. Zarka, and M. K. Dougherty (2016), Planetary period oscillations in Saturn's magnetosphere: Coalescence and reversal of northern and southern periods in late northern spring, *J. Geophys. Res. Space Physics*, *121*, 9829–9862, doi:10.1002/2016JA023056.

Sandel, B. R., and A. L. Broadfoot (1981), Morphology of Saturn's aurora, *Nature*, *292*, 679–682, doi:10.1038/292679a0.

Sandel, B. R., et al. (1982), Extreme ultraviolet observations from the Voyager 2 encounter with Saturn, *Science*, *215*, 548–553, doi:10.1126/science.215.4532.548.

Southwood, D. J., and M. G. Kivelson (2007), Saturn magnetospheric dynamics: Elucidation of a camshaft model, *J. Geophys. Res.*, *112*, A12222, doi:10.1029/2007JA012254.

Szego, K., Z. Nemeth, G. Erdos, L. Foldy, Z. Bebesi, M. Thomsen, and D. Delapp (2012), Location of the magnetodisk in the nightside outer magnetosphere of Saturn near equinox based on ion densities, *J. Geophys. Res.*, *117*, A09225, doi:10.1029/2012JA017817.

Szego, K., Z. Nemeth, L. Foldy, S. W. H. Cowley, and G. Provan (2013), Dual periodicities in the flapping of Saturn's magnetodisk, *J. Geophys. Res. Space Physics*, *118*, 2883–2887, doi:10.1002/jgra.50316.

Thomsen, M. F., C. M. Jackman, S. W. H. Cowley, X. Jia, M. G. Kivelson, and G. Provan (2017), Evidence for periodic variations in the thickness of Saturn's nightside plasma sheet, *J. Geophys. Res. Space Physics*, *122*, 280–292, doi:10.1002/2016JA023368.

Wang, Z., D. A. Gurnett, G. Fischer, S.-Y. Ye, W. S. Kurth, D. G. Mitchell, J. S. Leisner, and C. T. Russell (2010), Cassini observations of narrowband radio emissions in Saturn's magnetosphere, *J. Geophys. Res.*, *115*, A06213, doi:10.1029/2009JA014847.

Warwick, J. W., et al. (1981), Planetary radio astronomy observations from Voyager-1 near Saturn, *Science*, *212*, 239–243, doi:10.1126/science.212.4491.239.

Warwick, J. W., D. S. Evans, J. H. Romig, J. K. Alexander, M. D. Desch, M. L. Kaiser, M. Aubier, Y. Leblanc, A. Lecacheux, and B. M. Pedersen (1982), Planetary radio astronomy observations from Voyager-2 near Saturn, *Science*, *215*, 582–587, doi:10.1126/science.215.4532.582.

Ye, S.-Y., D. A. Gurnett, J. B. Groene, Z. Wang, and W. S. Kurth (2010), Dual periodicities in the rotational modulation of Saturn narrowband emissions, *J. Geophys. Res.*, *115*, A12258, doi:10.1029/2010JA015780.